SPICE – Workshop

TG New Methods: Algorithms, Grid Generation, Code Library

18th - 20th July 2005

Munich, Germany

The ADER-DG method for the simulation of elastic wave propagation on unstructured meshes

Martin Käser*, Michael Dumbser*, Josep de la Puente§

* DICA, University of Trento
§ Geophysics, LMU München

Motivation

Why very high order schemes for elastic waves ?

• physical models of the subsurface become more and more detailed,
accurate computations of resulting synthetic seismograms become essential

model validation

Motivation

Why very high order schemes for elastic waves ?

• physical models of the subsurface become more and more detailed, accurate computations of resulting synthetic seismograms become essential

model validation

• understanding of misfit only possible with highly accurate numerical schemes

separation of errors

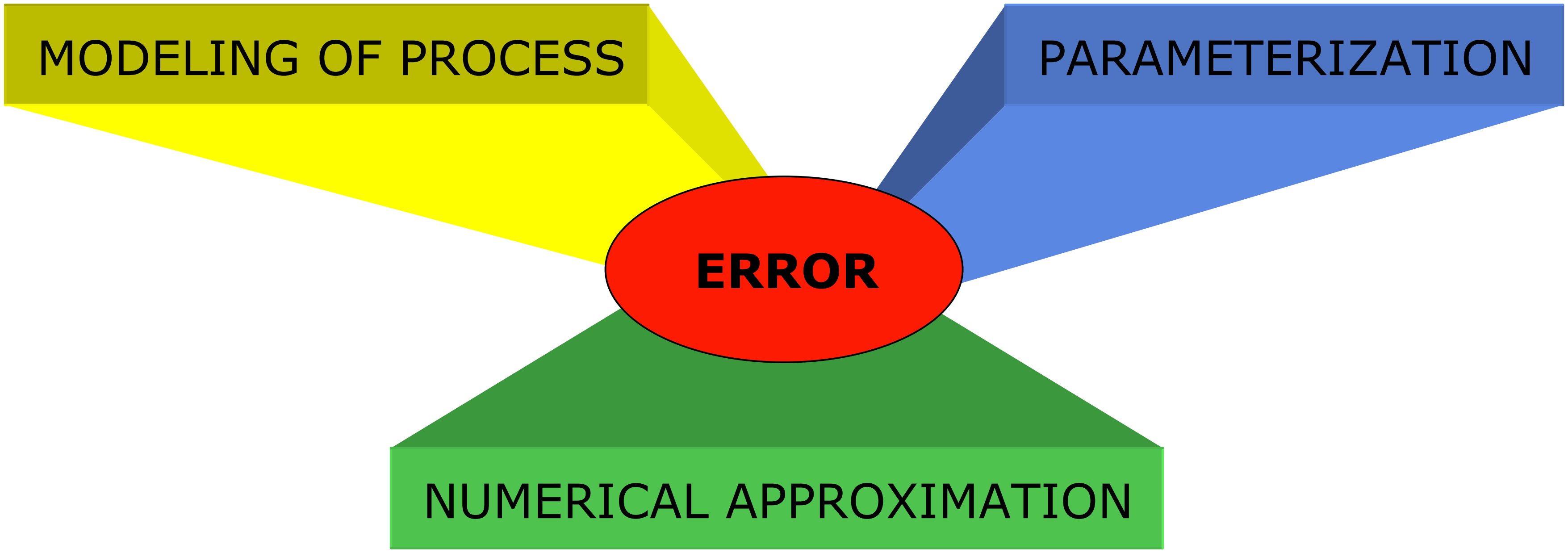

Motivation

Why very high order schemes for elastic waves ?

• physical models of the subsurface become more and more detailed, accurate computations of resulting synthetic seismograms become essential

model validation

• understanding of misfit only possible with highly accurate numerical schemes

separation of errors

• for wave propagation problems time accuracy is as important as space accuracy (amplitude and phase errors depend on time and space accuracy respectively)

space <u>AND</u> time accuracy

$$\frac{\partial}{\partial t}u + \frac{\partial}{\partial x}u = 0$$

Motivation

Why very high order schemes for elastic waves ?

• physical models of the subsurface become more and more detailed, accurate computations of resulting synthetic seismograms become essential

model validation

• understanding of misfit only possible with highly accurate numerical schemes

separation of errors

• for wave propagation problems time accuracy is as important as space accuracy (amplitude and phase errors depend on time and space accuracy respectively)

space <u>AND</u> time accuracy

• highly accurate numerical methods from the CFD community are applicable

CFD developments

Elastic Wave Equations

theory of linear elasticity
(definition of strain, Hooke´s law)
+
Newton´s law
(acceleration through forces caused by stress)
=
velocity-stress formulation
(non-conservative hyperbolic system)

$$
\begin{aligned}
\frac{\partial}{\partial t}\sigma_{xx} - (\lambda+2\mu)\frac{\partial}{\partial x}u - \lambda\frac{\partial}{\partial y}v - \lambda\frac{\partial}{\partial z}w &= 0\,,\\
\frac{\partial}{\partial t}\sigma_{yy} - \lambda\frac{\partial}{\partial y}v - (\lambda+2\mu)\frac{\partial}{\partial y}v - \lambda\frac{\partial}{\partial z}w &= 0\,,\\
\frac{\partial}{\partial t}\sigma_{zz} - \lambda\frac{\partial}{\partial x}u - \lambda\frac{\partial}{\partial y}v - (\lambda+2\mu)\frac{\partial}{\partial z}w &= 0\,,\\
\frac{\partial}{\partial t}\sigma_{xy} - \mu(\frac{\partial}{\partial x}v + \frac{\partial}{\partial y}u) &= 0\,,\\
\frac{\partial}{\partial t}\sigma_{xz} - \mu(\frac{\partial}{\partial z}u + \frac{\partial}{\partial x}w) &= 0\,,\\
\frac{\partial}{\partial t}\sigma_{yz} - \mu(\frac{\partial}{\partial z}v + \frac{\partial}{\partial y}w) &= 0\,,\\
\rho\frac{\partial}{\partial t}u - \frac{\partial}{\partial x}\sigma_{xx} - \frac{\partial}{\partial y}\sigma_{xy} - \frac{\partial}{\partial z}\sigma_{xz} &= 0\,,\\
\rho\frac{\partial}{\partial t}v - \frac{\partial}{\partial x}\sigma_{xy} - \frac{\partial}{\partial y}\sigma_{yy} - \frac{\partial}{\partial z}\sigma_{yz} &= 0\,,\\
\rho\frac{\partial}{\partial t}w - \frac{\partial}{\partial x}\sigma_{xz} - \frac{\partial}{\partial y}\sigma_{yz} - \frac{\partial}{\partial z}\sigma_{zz} &= 0\,.
\end{aligned}
$$

<u>In a heterogeneous medium:</u>

space-dependent material coefficients

Lame constants: $\lambda = \lambda(x,y,z)$,

$\mu = \mu(x,y,z)$,

density $\rho = \rho(x,y,z)$

Eigenstructure of the Hyperbolic System

Compact vector-matrix notation gives

$$\frac{\partial Q}{\partial t} + A\frac{\partial}{\partial x}Q + B\frac{\partial}{\partial y}Q + C\frac{\partial}{\partial z}Q = 0,$$

with the vector of unknowns and Jacobian matrices

$$Q = \begin{pmatrix} \sigma_{xx} \\ \sigma_{yy} \\ \sigma_{zz} \\ \sigma_{xy} \\ \sigma_{xz} \\ \sigma_{yz} \\ u \\ v \\ w \end{pmatrix}, \qquad A = \begin{pmatrix} 0 & 0 & 0 & 0 & 0 & 0 & -(\lambda+2\mu) & 0 & 0 \\ 0 & 0 & 0 & 0 & 0 & 0 & -\lambda & 0 & 0 \\ 0 & 0 & 0 & 0 & 0 & 0 & -\lambda & 0 & 0 \\ 0 & 0 & 0 & 0 & 0 & 0 & 0 & -\mu & 0 \\ 0 & 0 & 0 & 0 & 0 & 0 & 0 & 0 & -\mu \\ 0 & 0 & 0 & 0 & 0 & 0 & 0 & 0 & 0 \\ -\frac{1}{\rho} & 0 & 0 & 0 & 0 & 0 & 0 & 0 & 0 \\ 0 & 0 & 0 & -\frac{1}{\rho} & 0 & 0 & 0 & 0 & 0 \\ 0 & 0 & 0 & 0 & 0 & -\frac{1}{\rho} & 0 & 0 & 0 \end{pmatrix}$$

Eigenstructure (continued)

Eigenvalues give wave speeds of P- and S-waves

$$\begin{array}{lll} s_1 = -c_p, & s_2 = -c_s, & s_3 = -c_s, \\ s_4 = 0, & s_5 = 0, & s_6 = 0, \\ s_7 = c_s, & s_8 = c_s, & s_9 = c_p \end{array} \quad \text{with} \quad c_p = \sqrt{\frac{\lambda + 2\mu}{\rho}}, \quad c_s = \sqrt{\frac{\mu}{\rho}}$$

P-wave S-wave

Eigenvectors are given through

$$R_A = \begin{pmatrix} \lambda + 2\mu & 0 & 0 & 0 & 0 & 0 & 0 & 0 & \lambda + 2\mu \\ \lambda & 0 & 0 & 1 & 0 & 0 & 0 & 0 & \lambda \\ \lambda & 0 & 0 & 0 & 1 & 0 & 0 & 0 & \lambda \\ 0 & 0 & \mu & 0 & 0 & 0 & \mu & 0 & 0 \\ 0 & 0 & 0 & 0 & 0 & 1 & 0 & 0 & 0 \\ 0 & \mu & 0 & 0 & 0 & 0 & 0 & \mu & 0 \\ c_p & 0 & 0 & 0 & 0 & 0 & 0 & 0 & -c_p \\ 0 & 0 & c_s & 0 & 0 & 0 & -c_s & 0 & 0 \\ 0 & c_s & 0 & 0 & 0 & 0 & 0 & -c_s & 0 \end{pmatrix}$$

Discontinuous Galerkin (DG) Approach

(Reed & Hill, 1973; Cockburn & Shu, 1989, 1991)

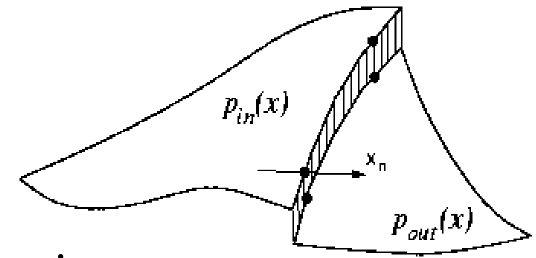

Ideas:

- piecewise polynomial approximation of unknown functions on **unstructured triangular** or **tetrahedral meshes**
- incorporation of well-established concepts of numerical **fluxes across element interfaces** into the finite element framework
- time evolution of **polynomial coefficients** (no point values or cell averages!) → no reconstruction or stencils !
- computations done on **reference element** → increase of computational efficiency !
- well-suited for **parallelization** due to **local** character of the scheme

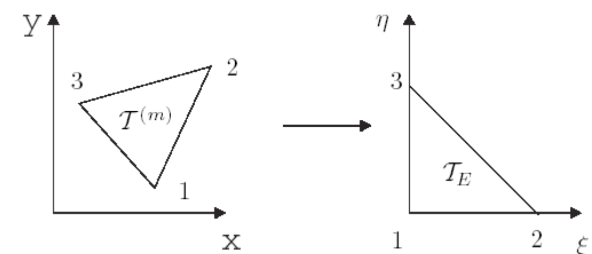

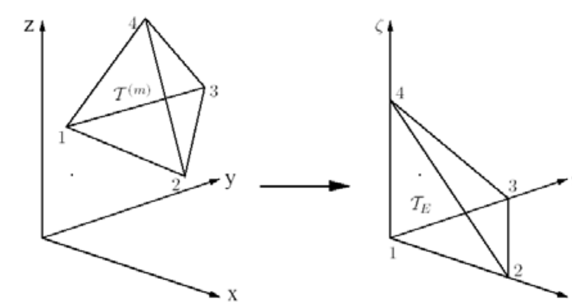

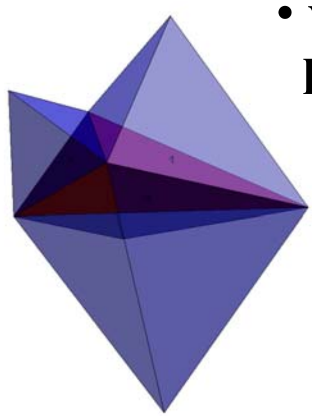

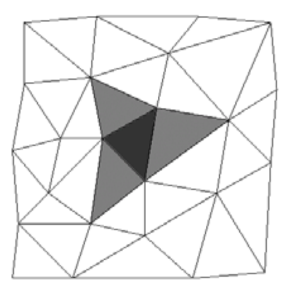

DG – The Numerical Scheme for 2-D

(Reed & Hill, 1973; Cockburn & Shu, 1989, 1991)

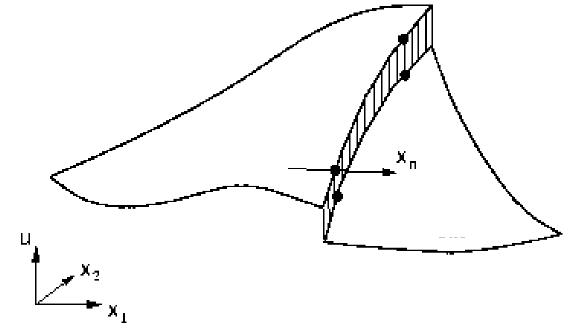

The governing system of equations is given by

$$\frac{\partial u_p}{\partial t} + A_{pq}\frac{\partial u_q}{\partial x} + B_{pq}\frac{\partial u_q}{\partial y} = 0,$$

Representation of the numerical approximation of the state vector u_h in element (m) in terms of l basis functions Φ

$$\left(u_h^{(m)}\right)_p(\xi,\eta,t) = \hat{u}_{pl}^{(m)}(t)\Phi_l(\xi,\eta)$$

Index notation: Summation from $l = 1$ to N_d where $N_d = (N+1)(N+2) / 2$ is the number of degrees of freedom and N the degree of the approximation polynomial

The basis functions Φ are combinations of Jacobi-polynomials and form an orthogonal basis on triangles and tetrahedrons.
Therefore, the mass matrix is always diagonal.

$$\Phi_0(\xi,\eta) = 1$$
$$\Phi_1(\xi,\eta) = -1 + 2\xi + \eta$$
$$\Phi_2(\xi,\eta) = -1 + 3\eta$$
$$\Phi_3(\xi,\eta) = \eta^2 - 2\eta + 6\xi\eta + 6\xi^2 - 6\xi + 1$$
$$\Phi_4(\xi,\eta) = 5\eta^2 - 6\eta + 10\xi\eta - 2\xi + 1$$
$$\Phi_5(\xi,\eta) = 10\eta^2 - 8\eta + 1$$

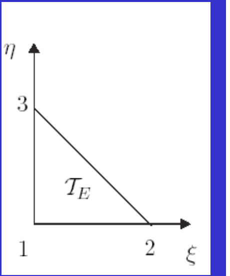

DG – The Numerical Scheme for 2-D

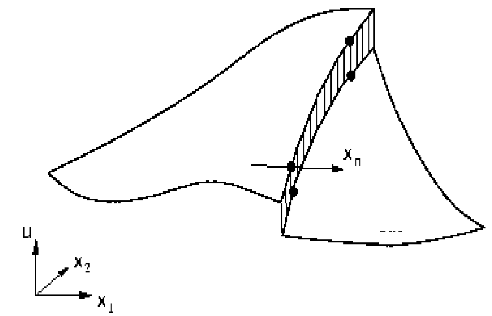

Multiplication of the governing equation with a test function Φ_k and integration over a triangle $\mathcal{T}^{(m)}$ gives

$$\int_{\mathcal{T}^{(m)}} \Phi_k \frac{\partial u_p}{\partial t} dV + \int_{\mathcal{T}^{(m)}} \Phi_k \left(A_{pq} \frac{\partial u_q}{\partial x} + B_{pq} \frac{\partial u_q}{\partial y} \right) dV = 0$$

Integration by parts yields

$$\int_{\mathcal{T}^{(m)}} \Phi_k \frac{\partial u_p}{\partial t} dV + \int_{\partial \mathcal{T}^{(m)}} \Phi_k F_p^h dS - \int_{\mathcal{T}^{(m)}} \left(\frac{\partial \Phi_k}{\partial x} A_{pq} u_q + \frac{\partial \Phi_k}{\partial y} B_{pq} u_q \right) dV = 0$$

The exact numerical flux in due to Roe´s method has the form

$$F_p^h = \frac{1}{2} T_{pq} \left(A_{qr}^{(m)} + \left| A_{qr}^{(m)} \right| \right) (T_{rs})^{-1} \hat{u}_{sl}^{(m)} \Phi_l^{(m)} + \frac{1}{2} T_{pq} \left(A_{qr}^{(m)} - \left| A_{qr}^{(m)} \right| \right) (T_{rs})^{-1} \hat{u}_{sl}^{(m_j)} \Phi_l^{(m_j)} ,$$

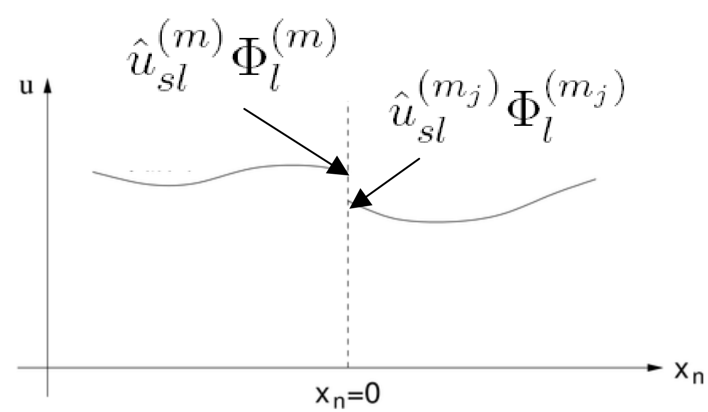

with

$$\left| A_{qr}^{(m)} \right| = R_{pr}^A \left| \Lambda_{rs} \right| \left(R_{sq}^A \right)^{-1} , \quad \text{with} \quad \left| \Lambda_{rs} \right| = \text{diag} \left(|s_1| , |s_2| , ... \right)$$

DG – The Numerical Scheme for 2-D

$$\int_{\mathcal{T}^{(m)}} \Phi_k \frac{\partial u_p}{\partial t} dV + \int_{\partial \mathcal{T}^{(m)}} \Phi_k F_p^h dS - \int_{\mathcal{T}^{(m)}} \left(\frac{\partial \Phi_k}{\partial x} A_{pq} u_q + \frac{\partial \Phi_k}{\partial y} B_{pq} u_q \right) dV = 0$$

Using the representation $u_p(\xi, \eta, t) = \hat{u}_{pl}^{(m)}(t) \Phi_l(\xi, \eta)$

and splitting the boundary integral into the flux contributions gives

$$\begin{aligned}
& \tfrac{\partial}{\partial t} \hat{u}_{pl}^{(m)} \int_{\mathcal{T}^{(m)}} \Phi_k \Phi_l dV \quad + \\
+ \quad & \sum_{j=1}^{3} T_{pq}^{j} \tfrac{1}{2} \left(A_{qr}^{(m)} + \left| A_{qr}^{(m)} \right| \right) (T_{rs}^{j})^{-1} \hat{u}_{sl}^{(m)} \int_{\left(\partial \mathcal{T}^{(m)}\right)_j} \Phi_k^{(m)} \Phi_l^{(m)} dS \quad + \\
+ \quad & \sum_{j=1}^{3} T_{pq}^{j} \tfrac{1}{2} \left(A_{qr}^{(m)} - \left| A_{qr}^{(m)} \right| \right) (T_{rs}^{j})^{-1} \hat{u}_{sl}^{(m_j)} \int_{\left(\partial \mathcal{T}^{(m)}\right)_j} \Phi_k^{(m)} \Phi_l^{(m_j)} dS \quad - \\
- \quad & A_{pq} \hat{u}_{ql}^{(m)} \int_{\mathcal{T}^{(m)}} \tfrac{\partial \Phi_k}{\partial x} \Phi_l dV - B_{pq} \hat{u}_{ql}^{(m)} \int_{\mathcal{T}^{(m)}} \tfrac{\partial \Phi_k}{\partial y} \Phi_l dV \quad = \quad 0.
\end{aligned}$$

DG – The Numerical Scheme for 2-D

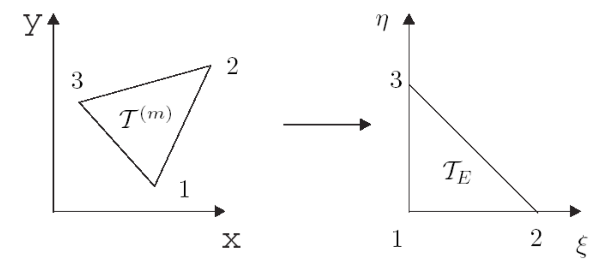

Transformation into the reference element is given through

$$\xi = \frac{1}{|J|}\left((x_3 y_1 - x_1 y_3) + x\,(y_3 - y_1) + y\,(x_1 - x_3)\right),$$

$$\eta = \frac{1}{|J|}\left((x_1 y_2 - x_2 y_1) + x\,(y_1 - y_2) + y\,(x_2 - x_1)\right),$$

$$x = x_1 + (x_2 - x_1)\,\xi + (x_3 - x_1)\,\eta,$$

$$y = y_1 + (y_2 - y_1)\,\xi + (y_3 - y_1)\,\eta,$$

with $|J| = (x_2 - x_1)(y_3 - y_1) - (x_3 - x_1)(y_2 - y_1)$

The Jacobian matrix of the transformation is given through $J = \begin{pmatrix} x_\xi & y_\xi \\ x_\eta & y_\eta \end{pmatrix}$ and it holds

$$dxdy = |J|\, d\xi d\eta, \qquad \begin{pmatrix} u_x \\ u_y \end{pmatrix} = J^{-1} \begin{pmatrix} u_\xi \\ u_\eta \end{pmatrix}$$

This provides the transformed Jacobian matrices of the governing equation as

$$A^*_{pq} = A_{pq}\frac{\partial \xi}{\partial x} + B_{pq}\frac{\partial \xi}{\partial y},$$

$$B^*_{pq} = A_{pq}\frac{\partial \eta}{\partial x} + B_{pq}\frac{\partial \eta}{\partial y}.$$

DG – The Numerical Scheme for 2-D

The transformation of the equation into the reference element then gives

$$\frac{\partial}{\partial t}\hat{u}_{pl}^{(m)}\,|J|\int_{\mathcal{T}_E}\Phi_k\Phi_l d\xi d\eta \quad +$$

$$+\sum_{j=1}^{3} T_{pq}^{j}\frac{1}{2}\left(A_{qr}^{(m)}+\left|A_{qr}^{(m)}\right|\right)(T_{rs}^{j})^{-1}\hat{u}_{sl}^{(m)}\,|S_j|\int_0^1\Phi_k^{(m)}(\chi_j)\Phi_l^{(m)}(\chi_j)d\chi_j \quad +$$

$$+\sum_{j=1}^{3} T_{pq}^{j}\frac{1}{2}\left(A_{qr}^{(m)}-\left|A_{qr}^{(m)}\right|\right)(T_{rs}^{j})^{-1}\hat{u}_{sl}^{(m_j)}\,|S_j|\int_0^1\Phi_k^{(m)}(\chi_j)\Phi_l^{(m_j)}(\chi_j)d\chi_j \, -$$

$$-A_{pq}^{*}\hat{u}_{ql}\,|J|\int_{\mathcal{T}_E}\frac{\partial\Phi_k}{\partial\xi}\Phi_l d\xi d\eta - B_{pq}^{*}\hat{u}_{ql}\,|J|\int_{\mathcal{T}_E}\frac{\partial\Phi_k}{\partial\eta}\Phi_l d\xi d\eta \quad = \quad 0$$

$0 \le \chi_j \le 1$ parameterizes the j-th edge of the reference triangle and

$|S_j|$ is its length in physical space

DG – The Numerical Scheme for 2-D

The transformation of the equation into the reference element then gives

$$
\begin{aligned}
&\frac{\partial}{\partial t}\hat{u}_{pl}^{(m)} \, |J| \int_{\mathcal{T}_E} \Phi_k \Phi_l d\xi d\eta \quad + \\
&+ \sum_{j=1}^{3} T_{pq}^{j} \frac{1}{2}\left(A_{qr}^{(m)} + \left|A_{qr}^{(m)}\right|\right)(T_{rs}^{j})^{-1} \hat{u}_{sl}^{(m)} \, |S_j| \int_0^1 \Phi_k^{(m)}(\chi_j)\Phi_l^{(m)}(\chi_j) d\chi_j \quad + \\
&+ \sum_{j=1}^{3} T_{pq}^{j} \frac{1}{2}\left(A_{qr}^{(m)} - \left|A_{qr}^{(m)}\right|\right)(T_{rs}^{j})^{-1} \hat{u}_{sl}^{(m_j)} \, |S_j| \int_0^1 \Phi_k^{(m)}(\chi_j)\Phi_l^{(m_j)}(\chi_j) d\chi_j \; - \\
&- A_{pq}^{*} \hat{u}_{ql} \, |J| \int_{\mathcal{T}_E} \frac{\partial \Phi_k}{\partial \xi} \Phi_l d\xi d\eta - B_{pq}^{*} \hat{u}_{ql} \, |J| \int_{\mathcal{T}_E} \frac{\partial \Phi_k}{\partial \eta} \Phi_l d\xi d\eta \quad = \quad 0
\end{aligned}
$$

The following integrals on the reference element can be pre-computed and stored

$$
\begin{aligned}
M_{kl} &= \int_{\mathcal{T}_E} \Phi_k \Phi_l d\xi d\eta, & K_{kl}^{\xi} &= \int_{\mathcal{T}_E} \frac{\partial \Phi_k}{\partial \xi} \Phi_l d\xi d\eta, \\
F_{kl}^{j,0} &= \int_0^1 \Phi_k^{(m)}(\chi_j)\Phi_l^{(m)}(\chi_j) d\chi_j, & K_{kl}^{\eta} &= \int_{\mathcal{T}_E} \frac{\partial \Phi_k}{\partial \eta} \Phi_l d\xi d\eta. \\
F_{kl}^{j,i} &= \int_0^1 \Phi_k^{(m)}(\chi_j)\Phi_l^{(m_j)}(\chi_j) d\chi_j, & &
\end{aligned}
$$

ADER-DG – Time Integration

The time integration over one time step from level n to n+1 leads to

$$\left[\left(\hat{u}_{pl}^{(m)}\right)^{n+1} - \left(\hat{u}_{pl}^{(m)}\right)^{n}\right] |J|\, M_{kl} \quad +$$

$$+ \quad \frac{1}{2}\sum_{j=1}^{3} T_{pq}^{j} \left(A_{qr}^{(m)} + \left|A_{qr}^{(m)}\right|\right) (T_{rs}^{j})^{-1} \left|S_j\right| F_{kl}^{j,0} \cdot I_{qlmn}(\Delta t) \left(\hat{u}_{mn}^{(m)}\right)^{n} +$$

$$+ \quad \frac{1}{2}\sum_{j=1}^{3} T_{pq}^{j} \left(A_{qr}^{(m)} - \left|A_{qr}^{(m)}\right|\right) (T_{rs}^{j})^{-1} \left|S_j\right| F_{kl}^{j,i} \cdot I_{qlmn}(\Delta t) \left(\hat{u}_{mn}^{(m_j)}\right)^{n} -$$

$$- \quad A_{pq}^{*} \,|J|\, K_{kl}^{\xi} \cdot I_{qlmn}(\Delta t) \left(\hat{u}_{mn}^{(m)}\right)^{n} - B_{pq}^{*} \,|J|\, K_{kl}^{\eta} \cdot I_{qlmn}(\Delta t) \left(\hat{u}_{mn}^{(m)}\right)^{n} = 0$$

where $\int_0^{\Delta t} \hat{u}_{pl}(t)dt = I_{plqm}(\Delta t)\hat{u}_{qm}(0)$ at local time level $t = t^n = 0$

ADER-DG – Time Integration

In the reference element we have the governing equation

$$\frac{\partial u_p}{\partial t} + A^*_{pq}\frac{\partial u_q}{\partial \xi} + B^*_{pq}\frac{\partial u_q}{\partial \eta} = 0$$

For a linear system the k-th time derivative is expressed by space derivatives

$$\frac{\partial^k u_p}{\partial t^k} = (-1)^k \left(A^*_{pq}\frac{\partial}{\partial \xi} + B^*_{pq}\frac{\partial}{\partial \eta} \right)^k u_q$$

The Taylor series expansion in time around u_p at local time level t=0 gives

$$u_p(\xi,\eta,t) = \sum_{k=0}^{N} \frac{t^k}{k!}\frac{\partial^k}{\partial t^k} u_p(\xi,\eta,0)$$

$$u_p(\xi,\eta,t) = \sum_{k=0}^{N} \frac{t^k}{k!}(-1)^k \left(A^*_{pq}\frac{\partial}{\partial \xi} + B^*_{pq}\frac{\partial}{\partial \eta} \right)^k \Phi_l(\xi,\eta)\hat{u}_{ql}(0)$$

ADER-DG – Time Integration

Projecting this approximation onto the basis functions gives the evolution of the degrees of freedom from level $t = t^n$ to $t^{n+1} = t^n + \Delta t$

$$\hat{u}_{pl}(t) = \frac{\left\langle \Phi_n, \sum_{k=0}^{N} \frac{t^k}{k!} (-1)^k \left(A^*_{pq} \frac{\partial}{\partial \xi} + B^*_{pq} \frac{\partial}{\partial \eta} \right)^k \Phi_m(\xi) \right\rangle}{\langle \Phi_n, \Phi_l \rangle} \hat{u}_{qm}(0)$$

Analytical time integration gives

$$\int_0^{\Delta t} \hat{u}_{pl}(t) dt = \frac{\left\langle \Phi_n, \sum_{k=0}^{N} \frac{\Delta t^{(k+1)}}{(k+1)!} (-1)^k \left(A^*_{pq} \frac{\partial}{\partial \xi} + B^*_{pq} \frac{\partial}{\partial \eta} \right)^k \Phi_m(\xi) \right\rangle}{\langle \Phi_n, \Phi_l \rangle} \hat{u}_{qm}(0)$$

where we define

$$I_{plqm}(\Delta t) = \frac{\left\langle \Phi_n, \sum_{k=0}^{N} \frac{\Delta t^{(k+1)}}{(k+1)!} (-1)^k \left(A^*_{pq} \frac{\partial}{\partial \xi} + B^*_{pq} \frac{\partial}{\partial \eta} \right)^k \Phi_m(\xi) \right\rangle}{\langle \Phi_n, \Phi_l \rangle}$$

Boundary Conditions

<u>Most important:</u> 1) open, outflow, absorbing, non-reflective boundaries
2) free surface boundaries

Open boundaries:

• only outgoing flux is considered, incoming flux is set to zero

$$F_p^{\text{OpenBC}} = \frac{1}{2} T_{pq} \left(A_{qr}^{(m)} + \left| A_{qr}^{(m)} \right| \right) (T_{rs})^{-1} \hat{u}_{sl}^{(m)} \Phi_l^{(m)}$$

Free surface boundaries:

• only outgoing flux is considered, incoming flux is set to zero

$$F_p^{\text{FreeBC}} = \frac{1}{2} T_{pq} \left(A_{qr}^{(m)} + \left| A_{qr}^{(m)} \right| \right) (T_{rs})^{-1} \hat{u}_{sl}^{(m)} \Phi_l^{(m)} + \frac{1}{2} T_{pq} \left(A_{qr}^{(m)} - \left| A_{qr}^{(m)} \right| \right) \Gamma_{rs} (T_{st})^{-1} \hat{u}_{tl}^{(m)} \Phi_l^{(m)}$$

with $\Gamma_{rs} = \text{diag}(-1, 1, -1, 1, 1)$

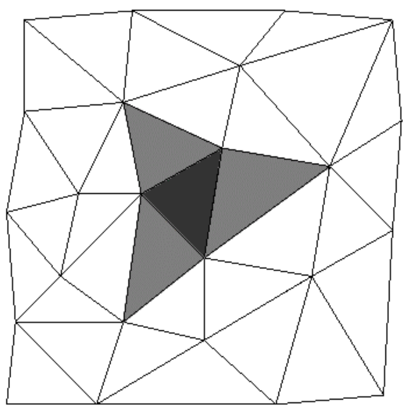

Numerical Accuracy and Convergence

- plane **P-** and **S-waves** travel with different speeds and in different directions
- after simulation time t = T waves **coincide with the initial condition**, i.e. $$Q_p(\vec{x},T) = Q_p(\vec{x},0)$$
- analysis up to **10-th order in space and time** on four mesh refinement levels on **regular** and **irregular** triangulations $$T = 100\sqrt{2},$$

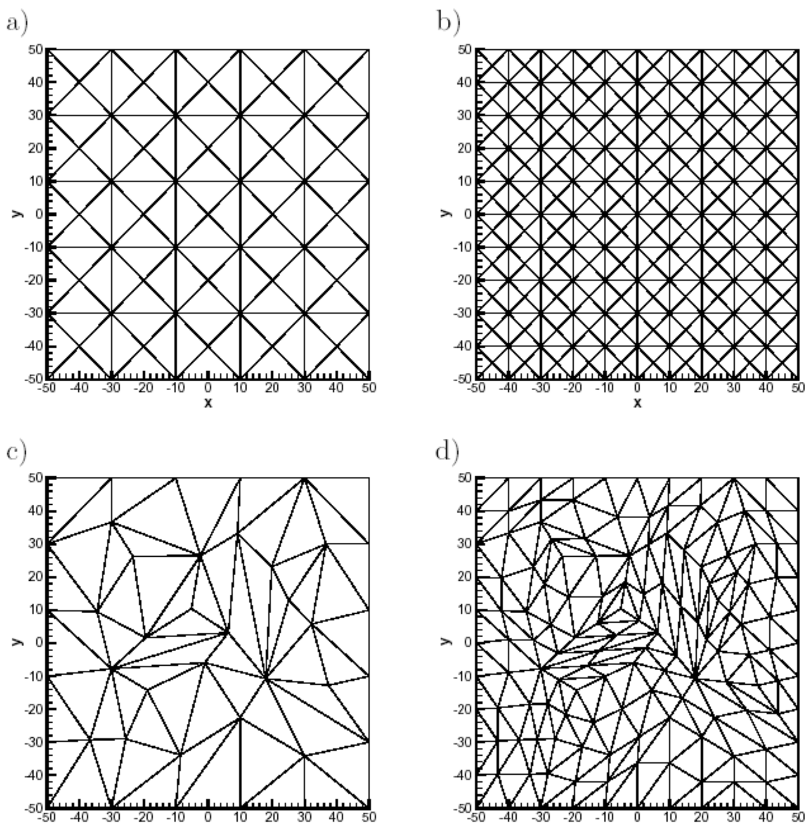

$$\lambda = 2, \qquad \mu = 1, \qquad \rho = 1,$$
$$c_p = 2, \qquad c_s = 1\,,$$

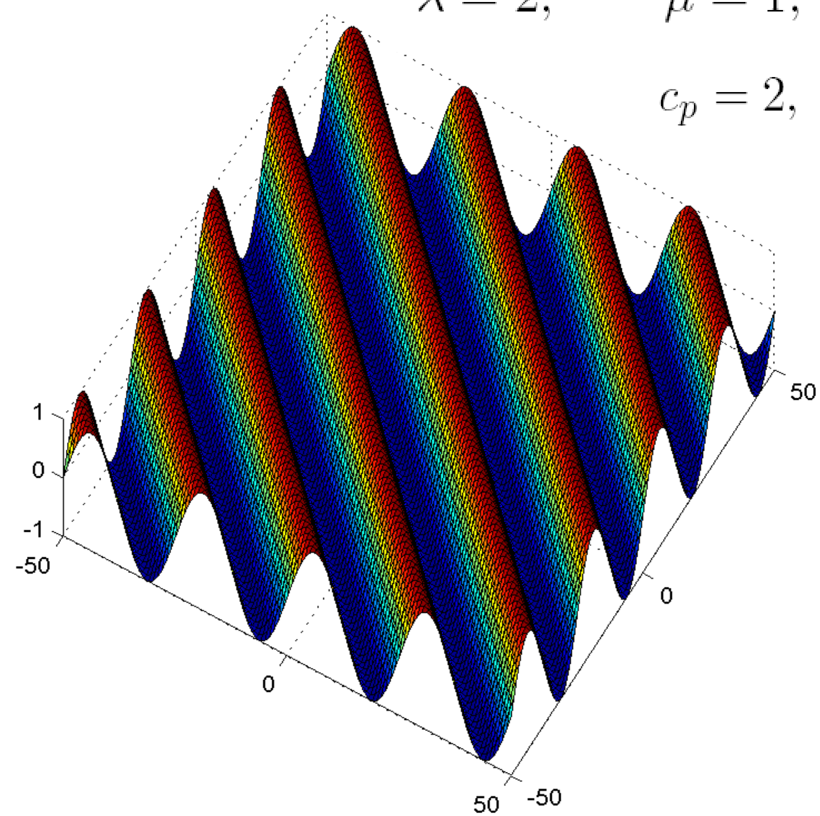

h	L^∞	$\mathcal{O}^\infty$	L^2	$\mathcal{O}^2$	N_d	CPU [s]
2.108	$1.542 \cdot 10^{0}$	–	$1.044 \cdot 10^{2}$	–	7500	123
1.054	$4.087 \cdot 10^{-1}$	1.916	$2.760 \cdot 10^{1}$	1.919	30000	892
0.703	$1.769 \cdot 10^{-1}$	2.065	$1.202 \cdot 10^{1}$	2.051	67500	2934
0.527	$9.733 \cdot 10^{-2}$	2.077	$6.657 \cdot 10^{0}$	2.053	120000	6925

Table 2: Convergence rates of ADER-DG $\mathcal{O}2$ on regular meshes.

h	L^∞	$\mathcal{O}^\infty$	L^2	$\mathcal{O}^2$	N_d	CPU [s]
3.514	$3.292 \cdot 10^{-2}$	–	$1.917 \cdot 10^{0}$	–	9000	147
2.108	$4.215 \cdot 10^{-3}$	4.024	$2.555 \cdot 10^{-1}$	3.945	25000	644
1.054	$2.734 \cdot 10^{-4}$	3.947	$1.633 \cdot 10^{-2}$	3.967	100000	4947
0.703	$5.444 \cdot 10^{-5}$	3.980	$3.243 \cdot 10^{-3}$	3.988	225000	16492

Table 4: Convergence rates of ADER-DG $\mathcal{O}4$ on regular meshes.

h	L^∞	$\mathcal{O}^\infty$	L^2	$\mathcal{O}^2$	N_d	CPU [s]
5.270	$2.003 \cdot 10^{-3}$	–	$7.847 \cdot 10^{-2}$	–	8400	221
2.635	$3.665 \cdot 10^{-5}$	5.772	$1.411 \cdot 10^{-3}$	5.797	33600	1650
1.757	$3.299 \cdot 10^{-6}$	5.938	$1.285 \cdot 10^{-4}$	5.909	75600	5437
1.318	$5.851 \cdot 10^{-7}$	6.012	$2.315 \cdot 10^{-5}$	5.959	134400	12730

Table 6: Convergence rates of ADER-DG $\mathcal{O}6$ on regular meshes.

h	L^∞	$\mathcal{O}^\infty$	L^2	$\mathcal{O}^2$	N_d	CPU [s]
5.270	$1.896 \cdot 10^{-5}$	–	$4.665 \cdot 10^{-4}$	–	14400	843
3.514	$8.074 \cdot 10^{-7}$	7.784	$1.955 \cdot 10^{-5}$	7.824	32400	2784
2.635	$7.903 \cdot 10^{-8}$	8.078	$2.010 \cdot 10^{-6}$	7.908	57600	6653
2.108	$1.365 \cdot 10^{-8}$	7.870	$3.449 \cdot 10^{-7}$	7.899	90000	12874

Table 8: Convergence rates of ADER-DG $\mathcal{O}8$ on regular meshes.

h	L^∞	$\mathcal{O}^\infty$	L^2	$\mathcal{O}^2$	N_d	CPU [s]
10.541	$8.902 \cdot 10^{-5}$	–	$1.660 \cdot 10^{-3}$	–	5500	381
5.270	$1.099 \cdot 10^{-7}$	9.662	$1.764 \cdot 10^{-6}$	9.879	22000	2878
3.514	$2.000 \cdot 10^{-9}$	9.882	$3.188 \cdot 10^{-8}$	9.898	49500	9946
2.635	$1.980 \cdot 10^{-10}$	8.038	$5.285 \cdot 10^{-9}$	6.246	88000	23100

Table 10: Convergence rates of ADER-DG $\mathcal{O}10$ on regular meshes.

h	L^∞	$\mathcal{O}^\infty$	L^2	$\mathcal{O}^2$	N_d	CPU [s]
6.513	$2.224 \cdot 10^{0}$	–	$1.459 \cdot 10^{2}$	–	2976	55
3.257	$1.201 \cdot 10^{0}$	0.889	$6.952 \cdot 10^{1}$	1.070	11904	438
1.628	$2.844 \cdot 10^{-1}$	2.078	$1.371 \cdot 10^{1}$	2.342	47616	3509
0.814	$5.748 \cdot 10^{-2}$	2.307	$2.704 \cdot 10^{0}$	2.342	190464	28232

Table 11: Convergence rates of ADER-DG $\mathcal{O}2$ on irregular meshes.

h	L^∞	$\mathcal{O}^\infty$	L^2	$\mathcal{O}^2$	N_d	CPU [s]
6.513	$1.447 \cdot 10^{-1}$	–	$1.768 \cdot 10^{0}$	–	9920	315
3.257	$1.111 \cdot 10^{-2}$	3.703	$9.910 \cdot 10^{-2}$	4.157	39680	2526
1.628	$1.054 \cdot 10^{-3}$	3.397	$6.604 \cdot 10^{-3}$	3.907	158720	20246
0.814	$8.002 \cdot 10^{-5}$	3.720	$4.266 \cdot 10^{-4}$	3.952	634880	164634

Table 13: Convergence rates of ADER-DG $\mathcal{O}4$ on irregular meshes.

h	L^∞	$\mathcal{O}^\infty$	L^2	$\mathcal{O}^2$	N_d	CPU [s]
13.026	$1.421 \cdot 10^{-1}$	–	$7.123 \cdot 10^{-1}$	–	5208	219
6.513	$3.845 \cdot 10^{-3}$	5.208	$1.279 \cdot 10^{-2}$	5.800	20832	1780
3.257	$6.839 \cdot 10^{-5}$	5.813	$2.255 \cdot 10^{-4}$	5.825	83328	14044
1.628	$1.220 \cdot 10^{-6}$	5.809	$3.892 \cdot 10^{-6}$	5.857	333312	107658

Table 15: Convergence rates of ADER-DG $\mathcal{O}6$ on irregular meshes.

h	L^∞	$\mathcal{O}^\infty$	L^2	$\mathcal{O}^2$	N_d	CPU [s]
26.052	$2.168 \cdot 10^{-1}$	–	$4.104 \cdot 10^{0}$	–	2232	111
13.026	$8.565 \cdot 10^{-3}$	4.662	$1.867 \cdot 10^{-2}$	7.780	8928	895
6.513	$4.746 \cdot 10^{-5}$	7.496	$9.682 \cdot 10^{-5}$	7.591	35712	7157
3.257	$2.154 \cdot 10^{-7}$	7.783	$4.058 \cdot 10^{-7}$	7.898	142848	57415

Table 17: Convergence rates of ADER-DG $\mathcal{O}8$ on irregular meshes.

h	L^∞	$\mathcal{O}^\infty$	L^2	$\mathcal{O}^2$	N_d	CPU [s]
26.052	$3.077 \cdot 10^{-2}$	–	$3.504 \cdot 10^{-1}$	–	3410	374
13.026	$2.393 \cdot 10^{-4}$	7.006	$3.241 \cdot 10^{-4}$	10.078	13640	2981
6.513	$3.265 \cdot 10^{-7}$	9.518	$5.065 \cdot 10^{-7}$	9.322	54560	23859
3.257	$4.330 \cdot 10^{-10}$	9.559	$6.134 \cdot 10^{-9}$	6.368	218240	191180

Table 19: Convergence rates of ADER-DG $\mathcal{O}10$ on irregular meshes.

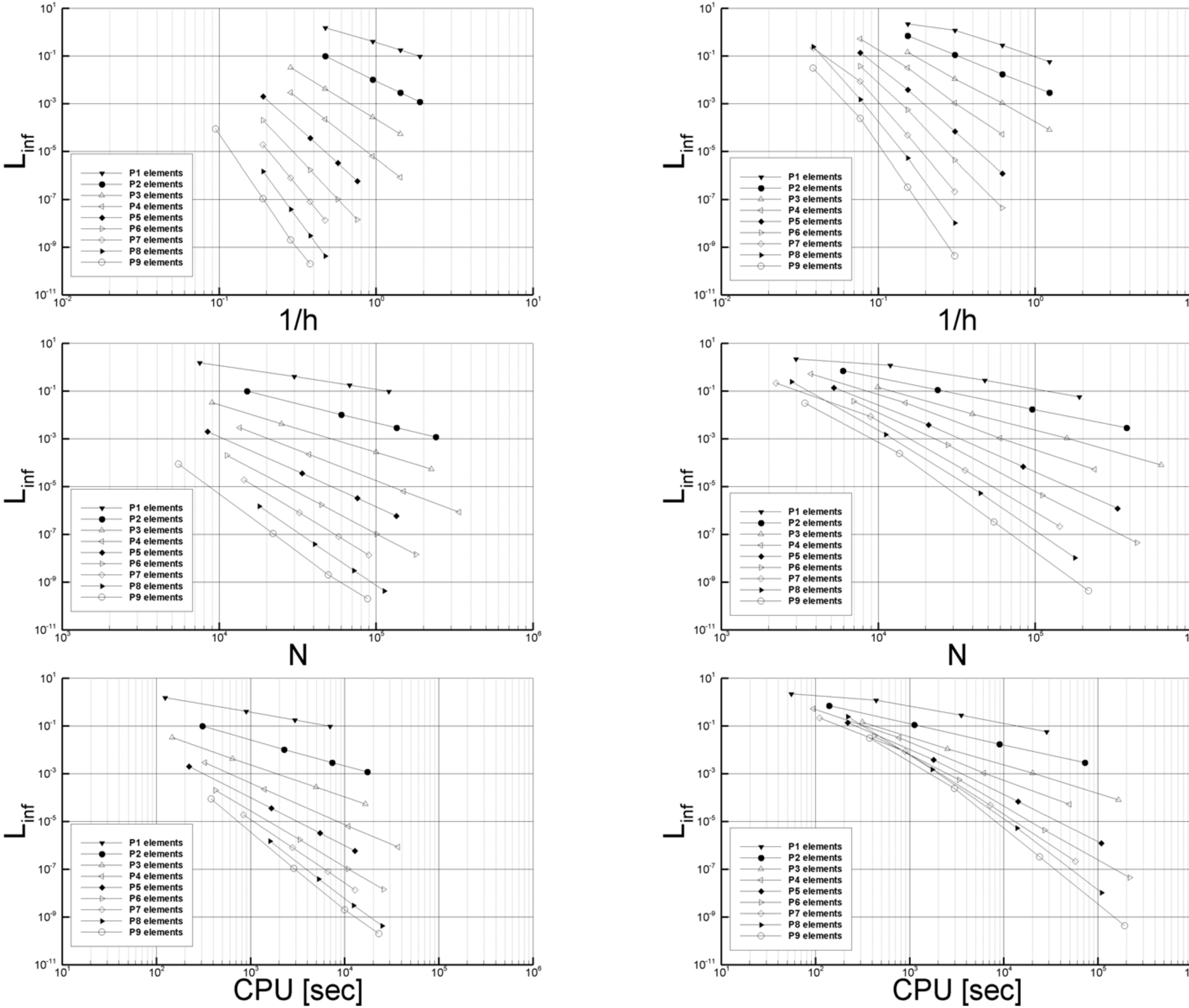
L_inf
1/h
N
CPU [sec]
P1 elements
P2 elements
P3 elements
P4 elements
P5 elements
P6 elements
P7 elements
P8 elements
P9 elements

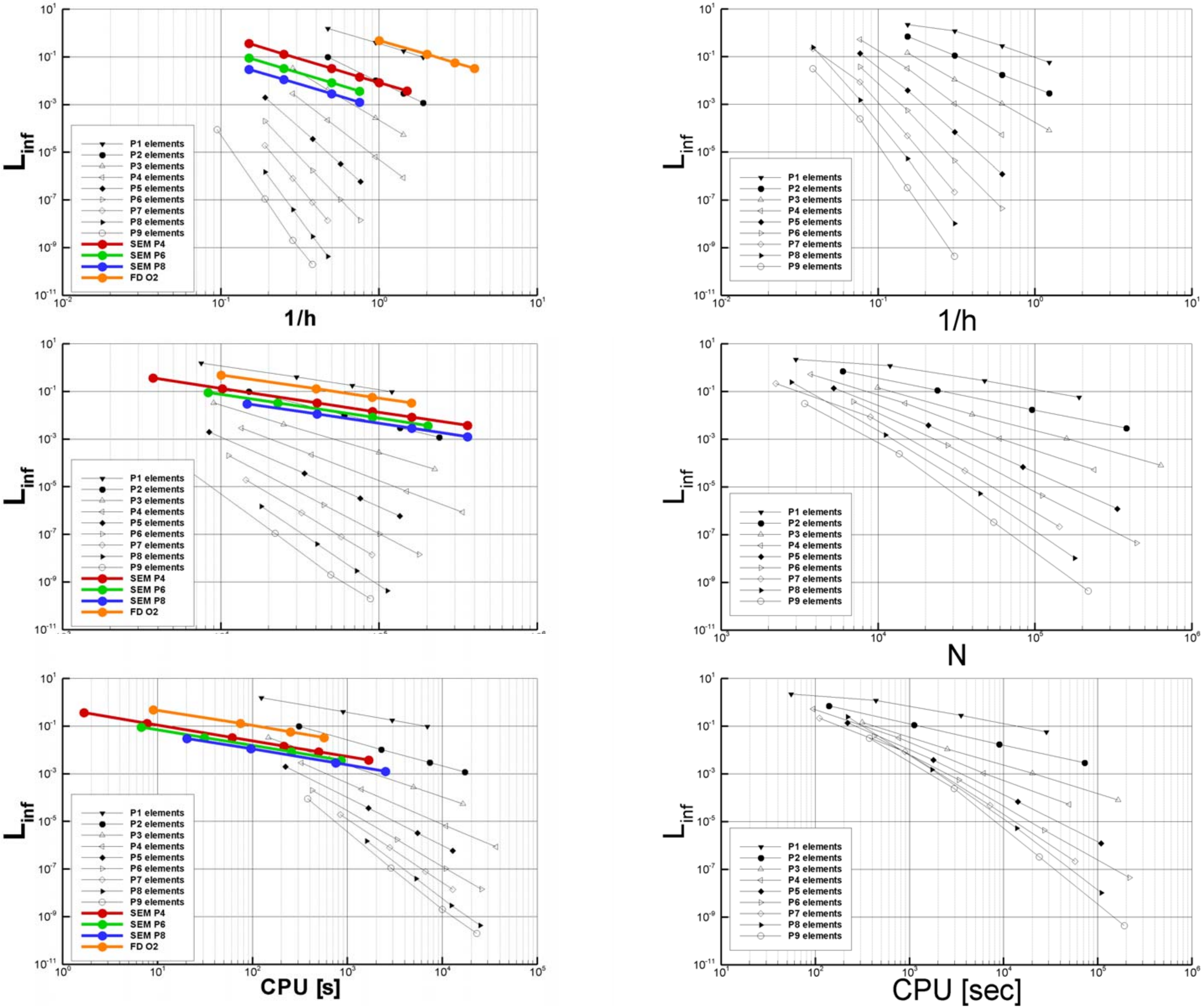

L_inf
1/h
P1 elements
P2 elements
P3 elements
P4 elements
P5 elements
P6 elements
P7 elements
P8 elements
P9 elements
SEM P4
SEM P6
SEM P8
FD O2
L_inf
1/h
P1 elements
P2 elements
P3 elements
P4 elements
P5 elements
P6 elements
P7 elements
P8 elements
P9 elements
L_inf
P1 elements
P2 elements
P3 elements
P4 elements
P5 elements
P6 elements
P7 elements
P8 elements
P9 elements
SEM P4
SEM P6
SEM P8
FD O2
L_inf
N
P1 elements
P2 elements
P3 elements
P4 elements
P5 elements
P6 elements
P7 elements
P8 elements
P9 elements
L_inf
CPU [s]
P1 elements
P2 elements
P3 elements
P4 elements
P5 elements
P6 elements
P7 elements
P8 elements
P9 elements
SEM P4
SEM P6
SEM P8
FD O2
L_inf
CPU [sec]
P1 elements
P2 elements
P3 elements
P4 elements
P5 elements
P6 elements
P7 elements
P8 elements
P9 elements

Application: Strong Material Contrasts

(LeVeque, 2002)

Order: 6 Mesh: 100 x 50 CPU time: 50%

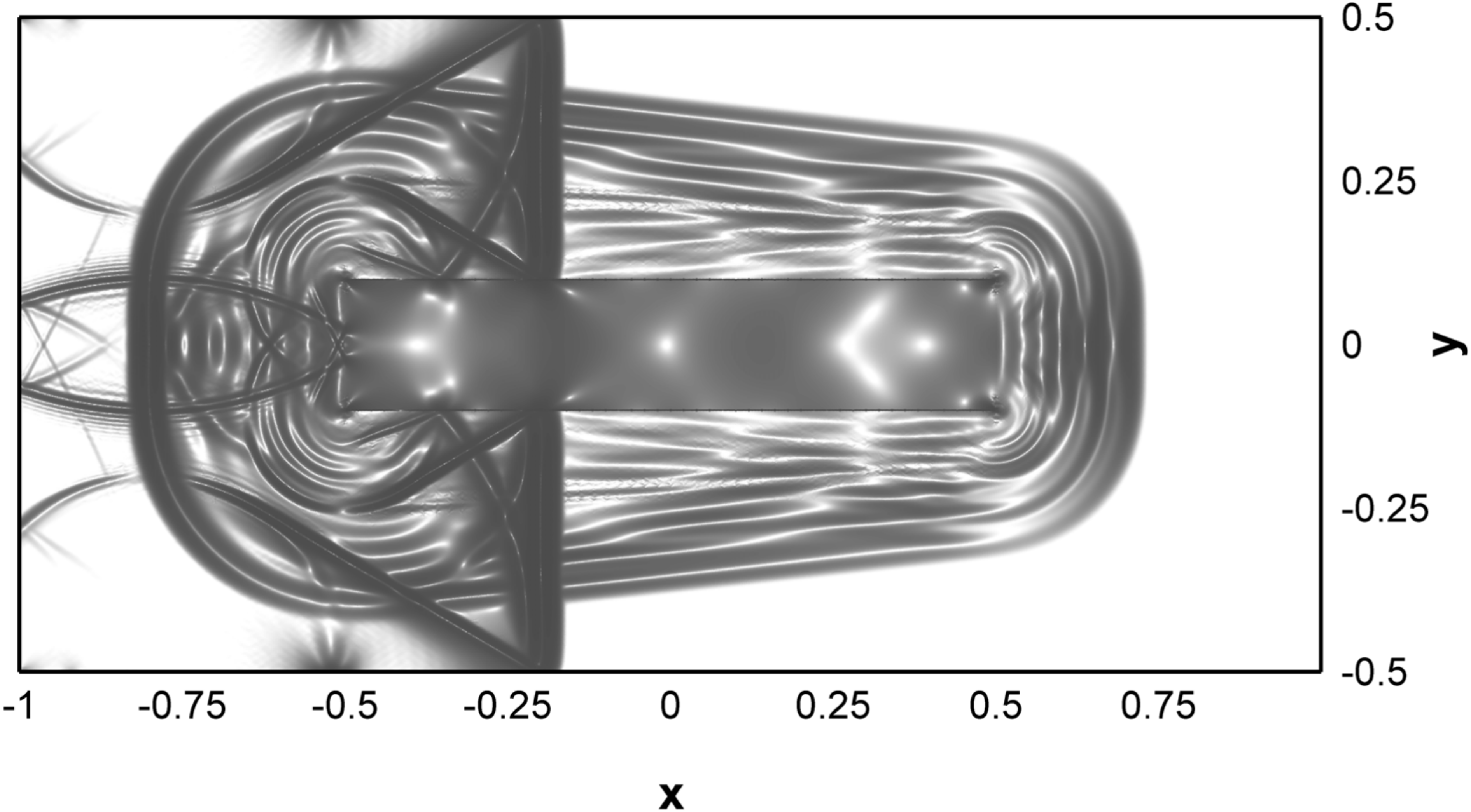

Application: Global Seismology using PREM

(Dziewonski & Anderson, 1981)

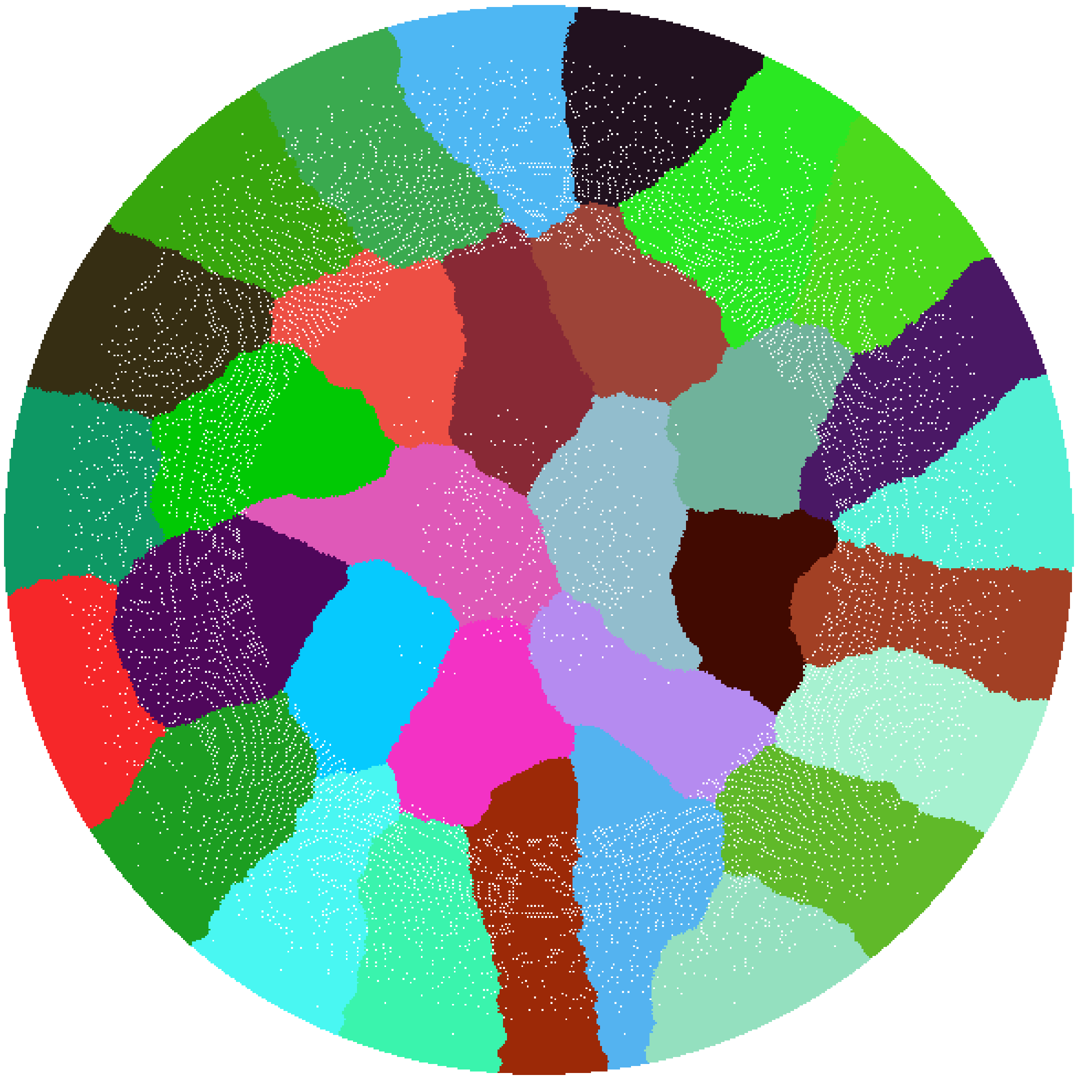

- triangular mesh adapts nicely to **geometry**
- mesh spacing **proportional to P-wave velocity**
- optimal use of the **CFL criterion**
- unphysical, **decreasing mesh spacing** towards the center is avoided
- **no** grid staggering
- **no** interpolation at hanging nodes
- **parallelization** with **METIS** mesh partitioning

Example: Global Seismology using PREM

(Dziewonski & Anderson, 1981)

vertical velocity component v $\qquad$ shear stress component σ_{xy}

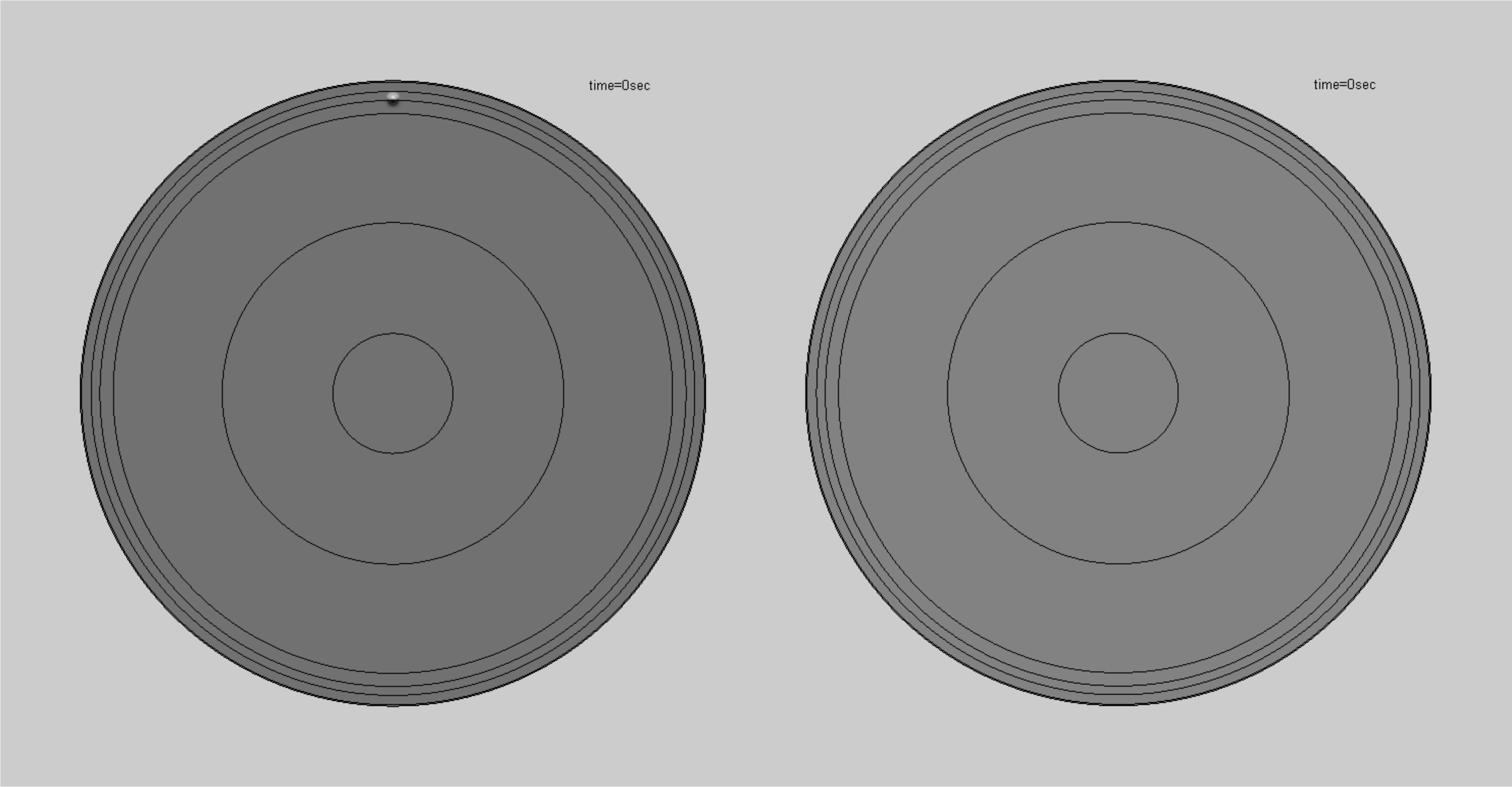

Free Surface Boundary (Lamb´s Problem)

(Lamb, 1904)

- vertical point force on the **free surface**
- investigation of accuracy of **P-**, **S-**, and **Rayleigh waves**
- setup similar to test case of

(D.Komatitsch & J.P.Vilotte, 1998)

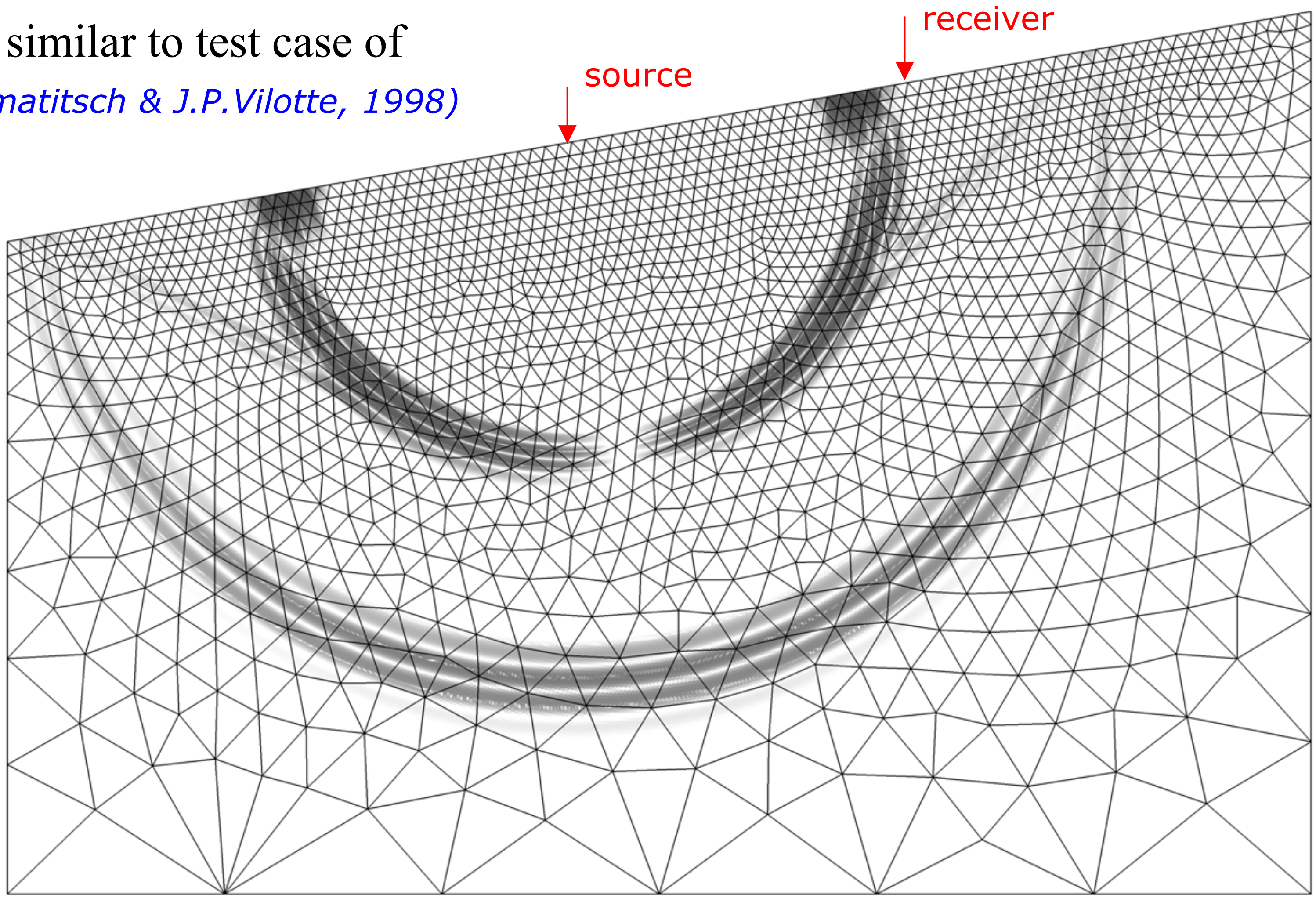

Free Surface Boundary (Lamb´s Problem)

(Lamb, 1904)

- vertical point force on the **free surface**
- investigation of accuracy of **P-**, **S-**, and **Rayleigh waves**
- setup similar to test case of

  (D.Komatitsch & J.P.Vilotte, 1998)

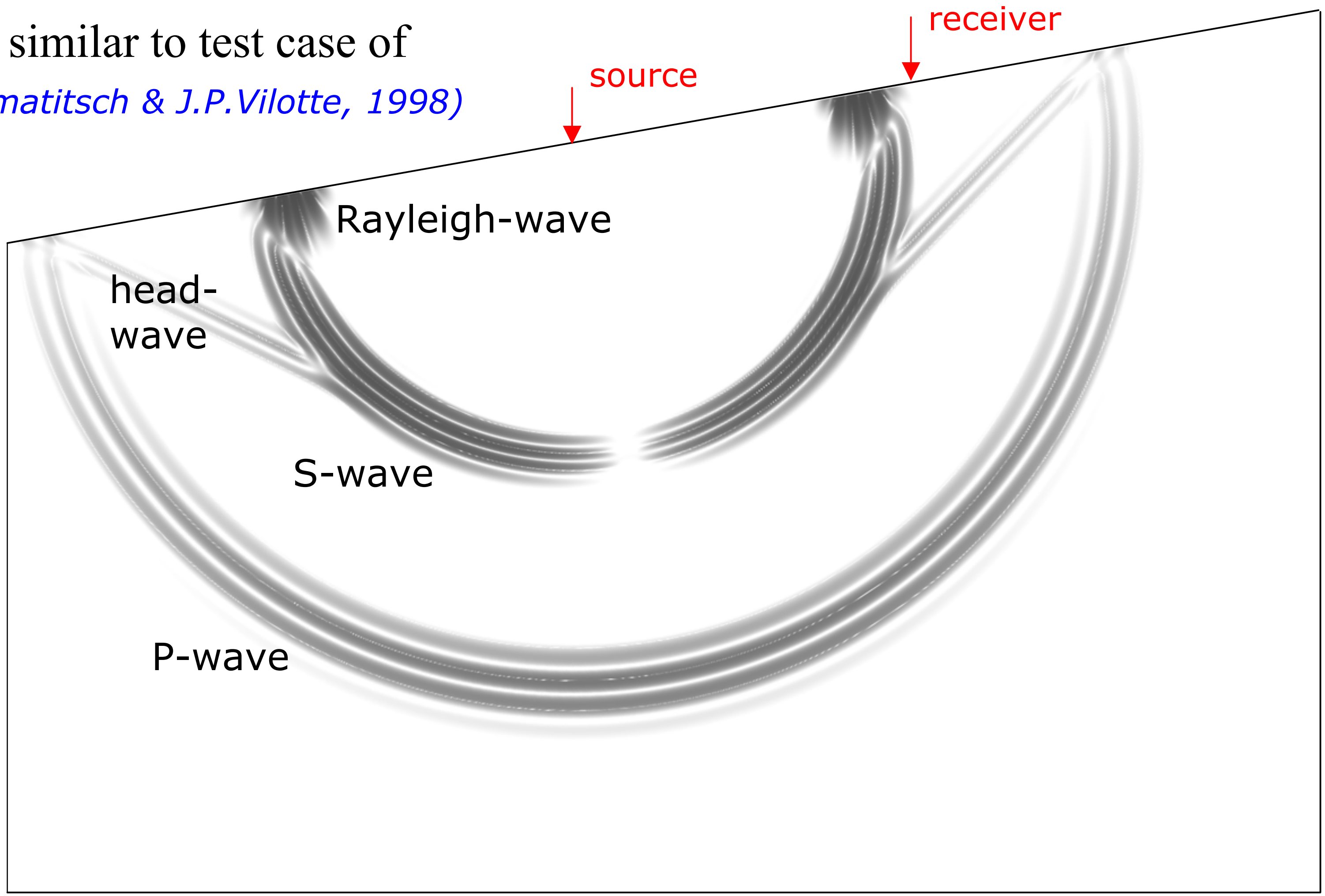

Free Surface Boundary (Lamb´s Problem)

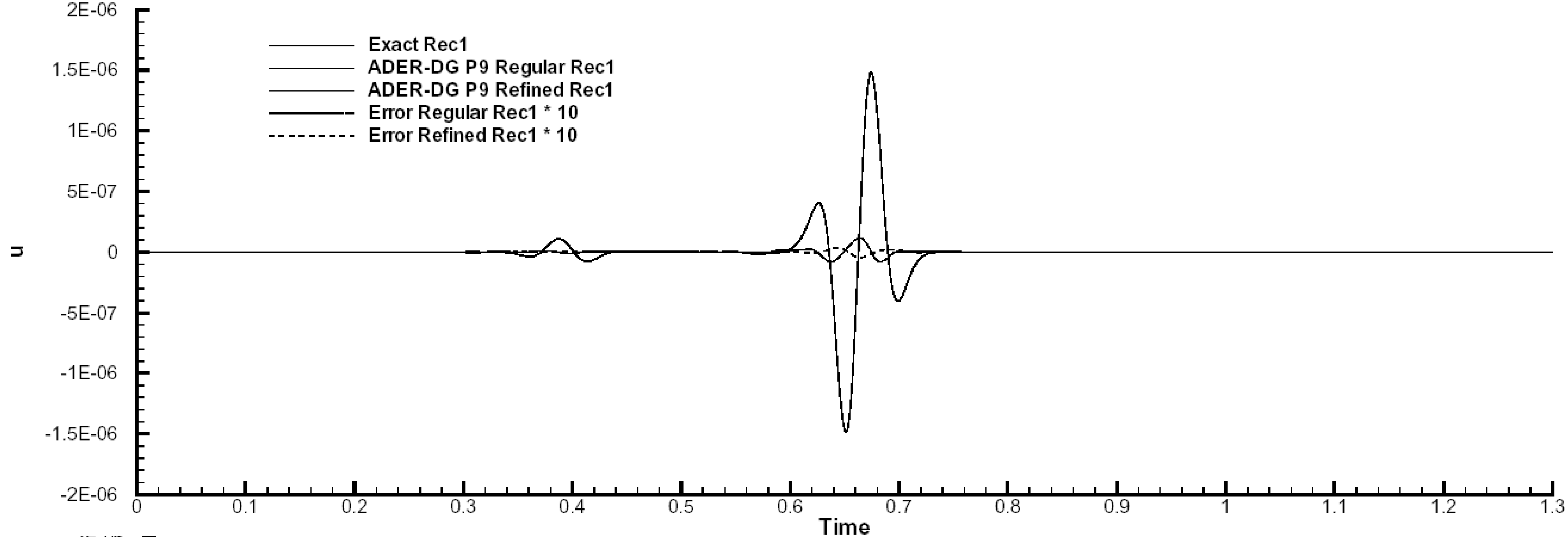

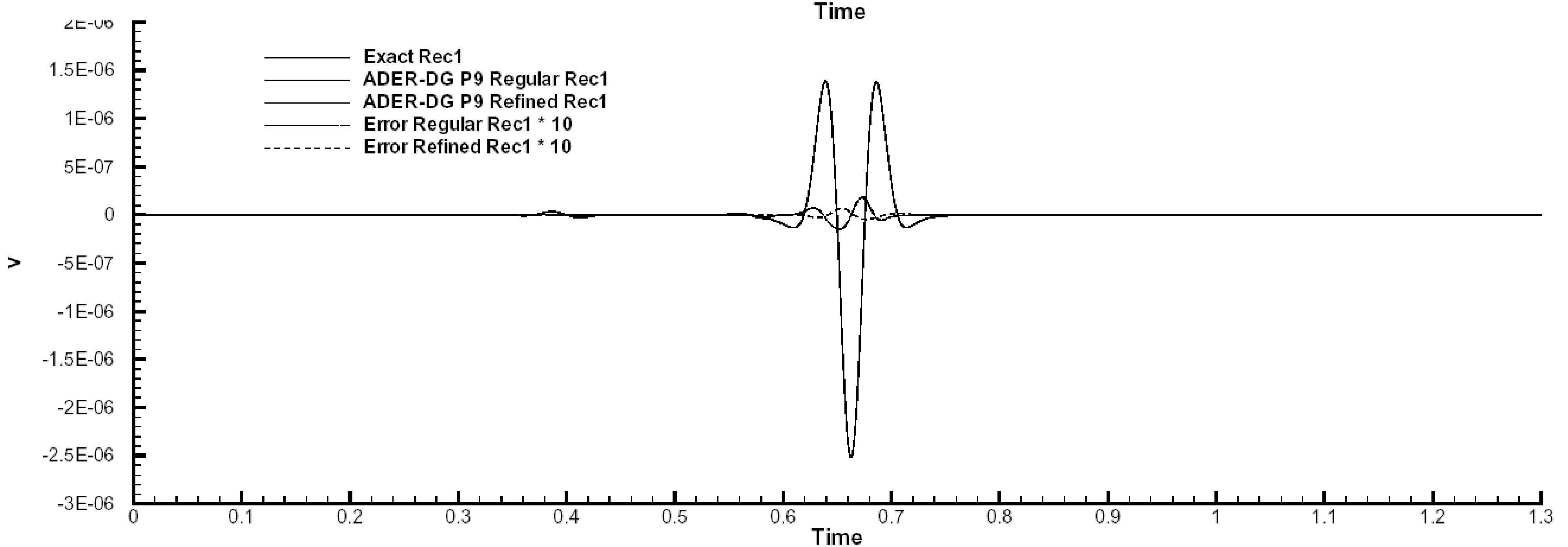

3-D Applications in Progress

- Tetraheral meshes give the **flexibility** needed for **complex geometries**
- **METIS** mesh partitioner can handle large 3-D tetrahedral meshes easily

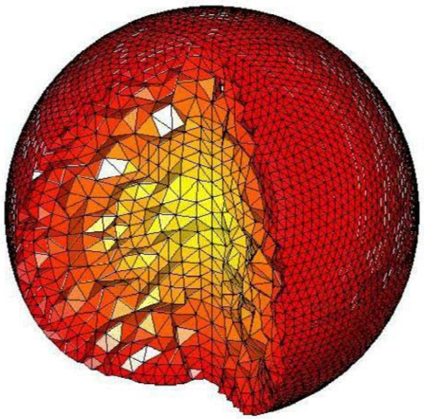

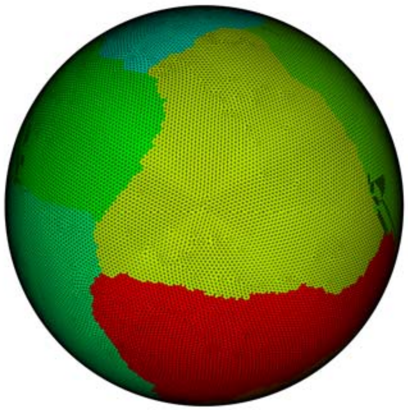

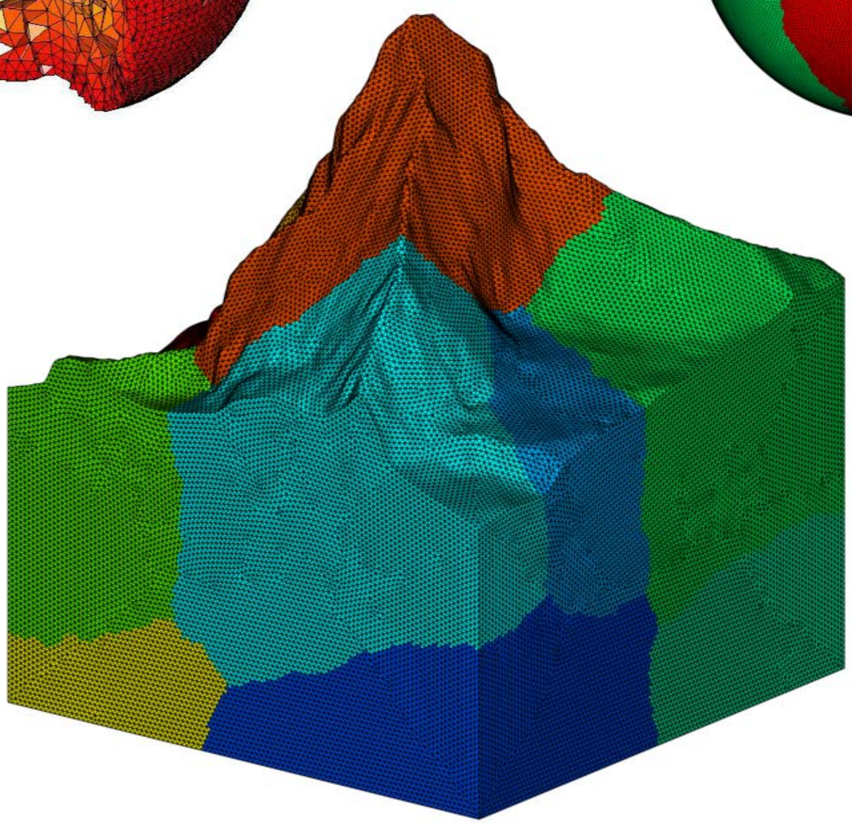

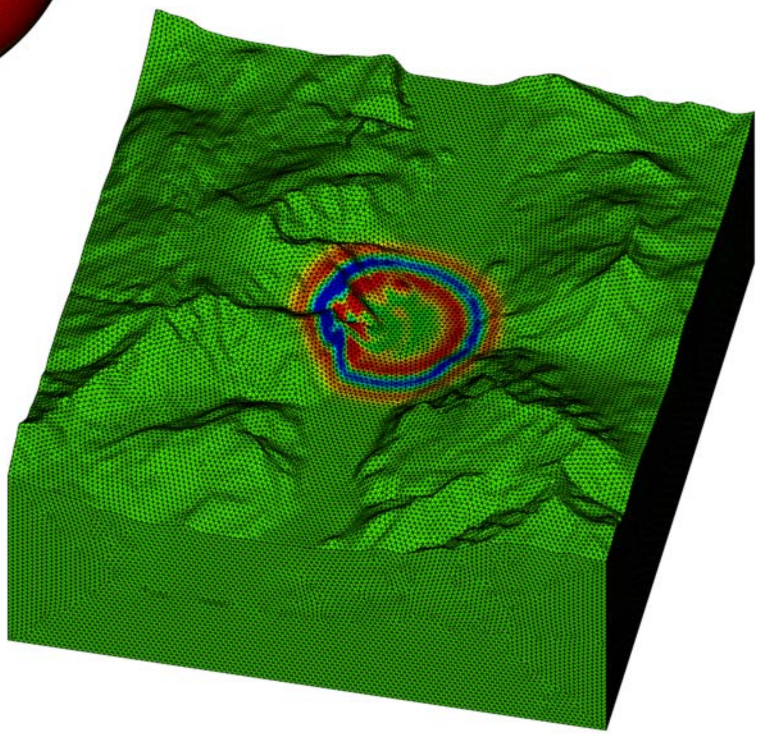


5500km

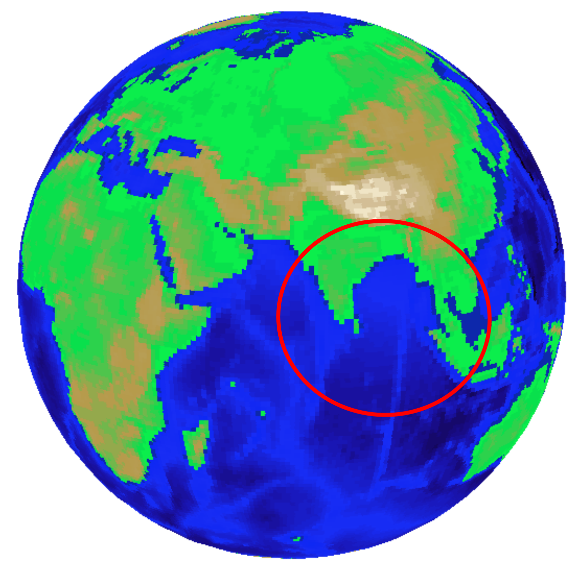

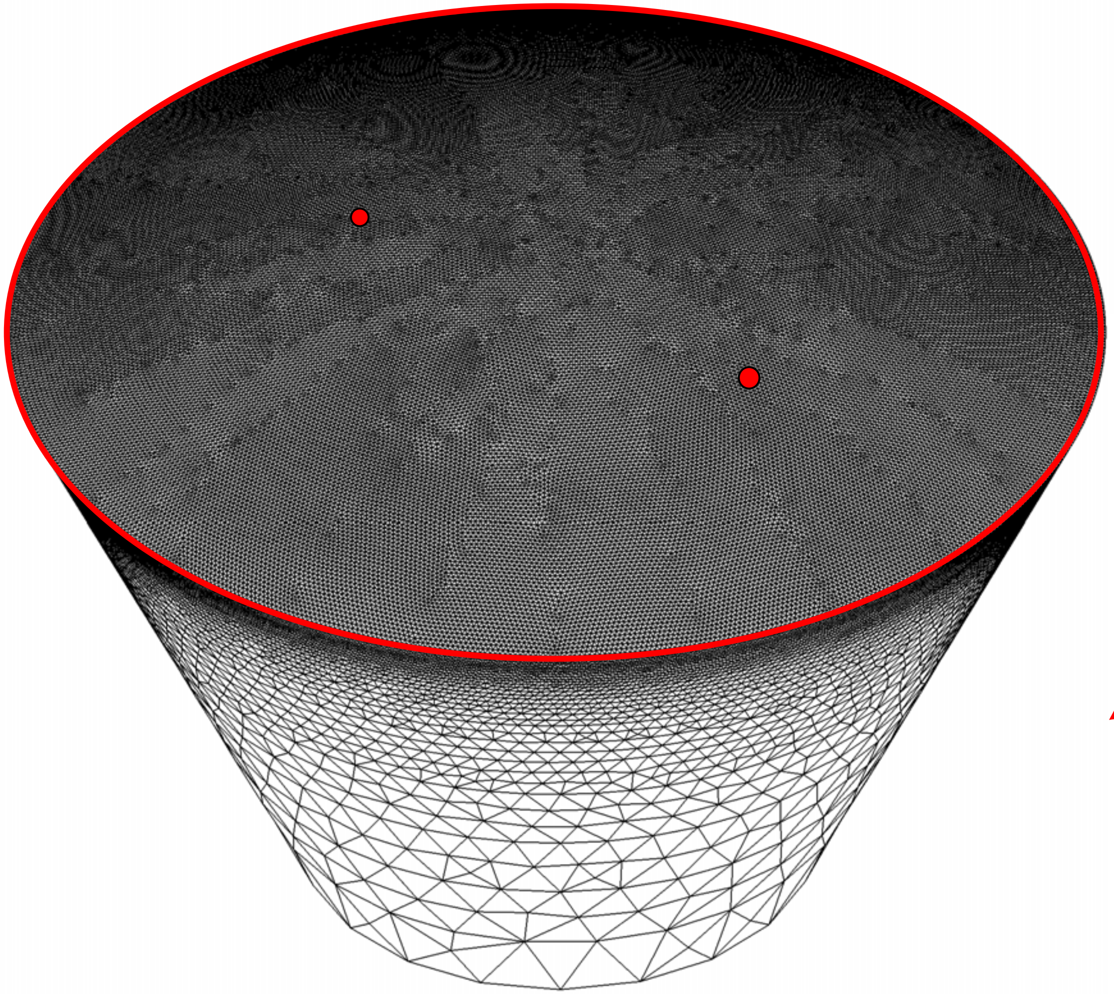

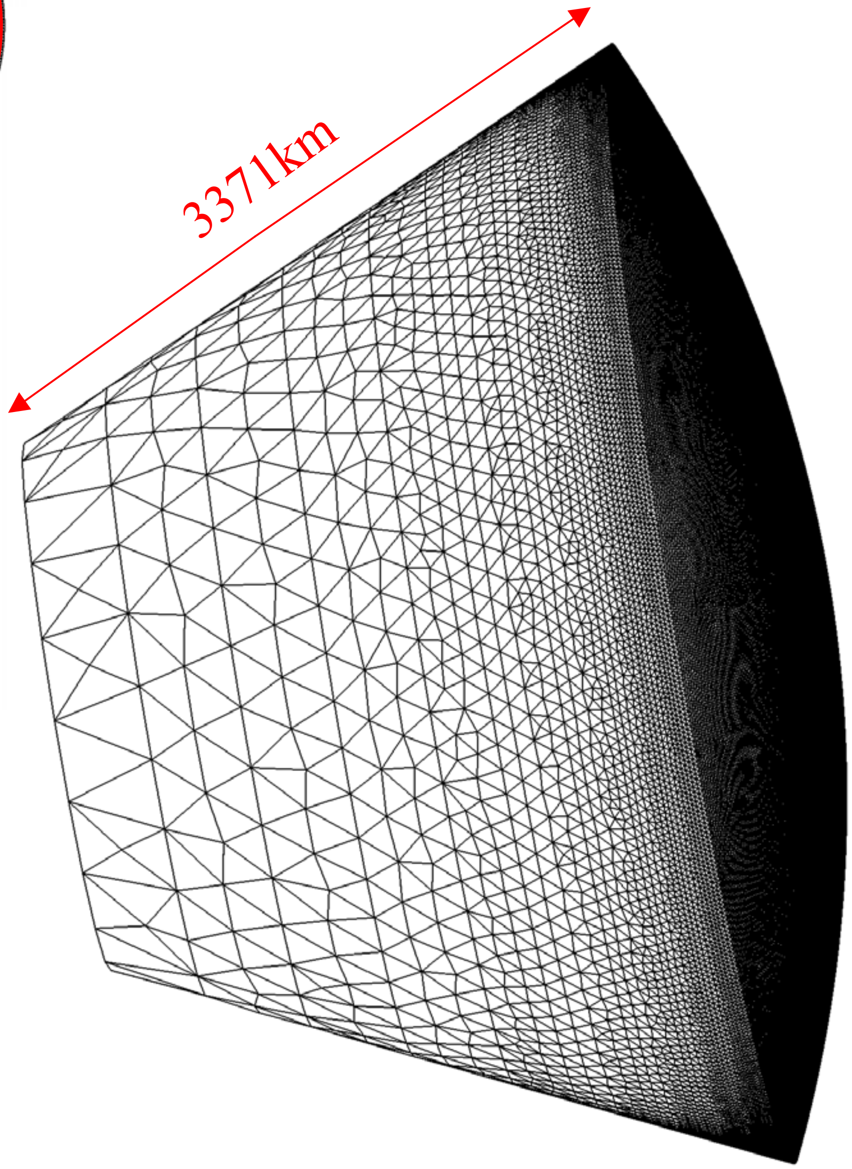
3371km

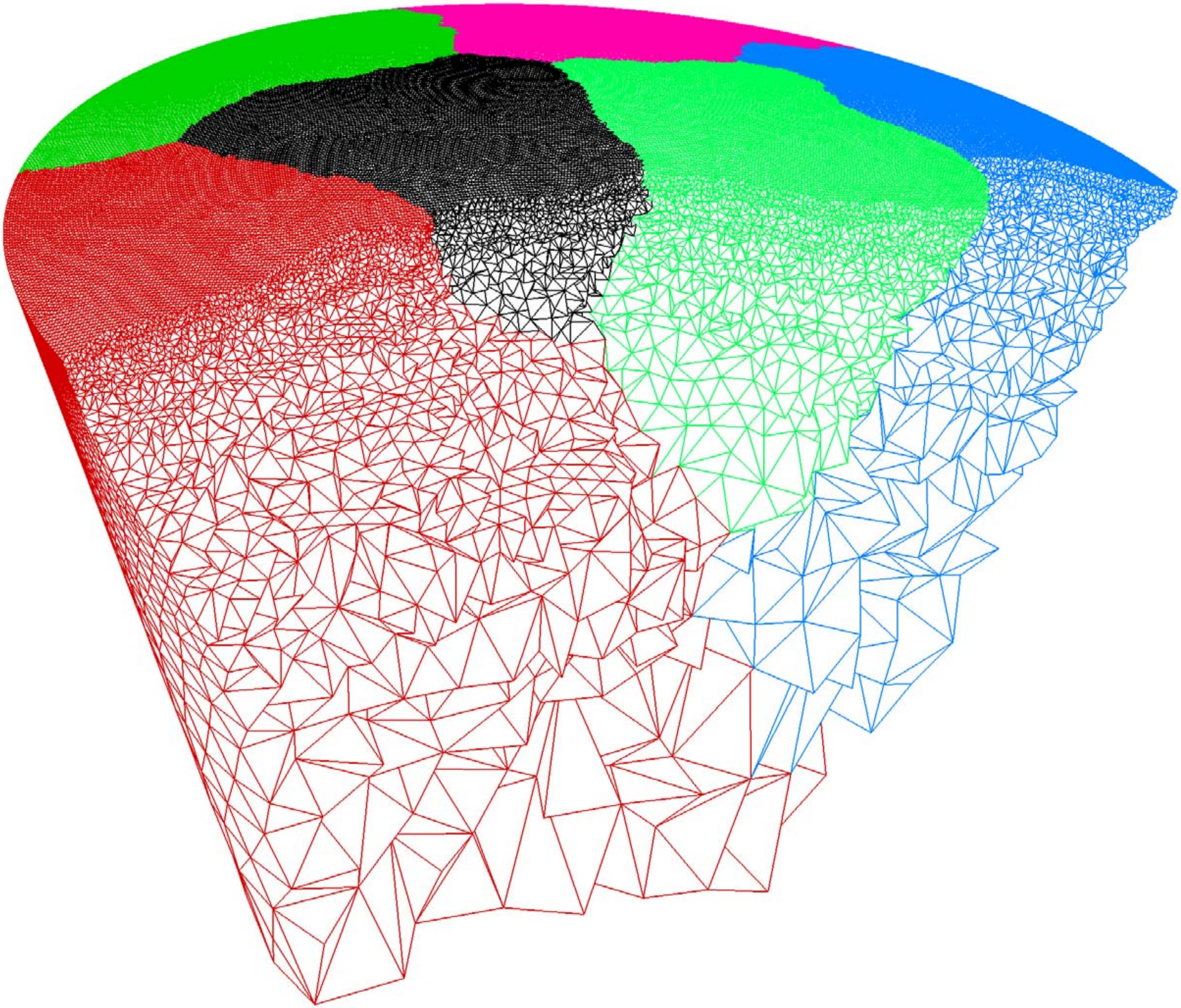

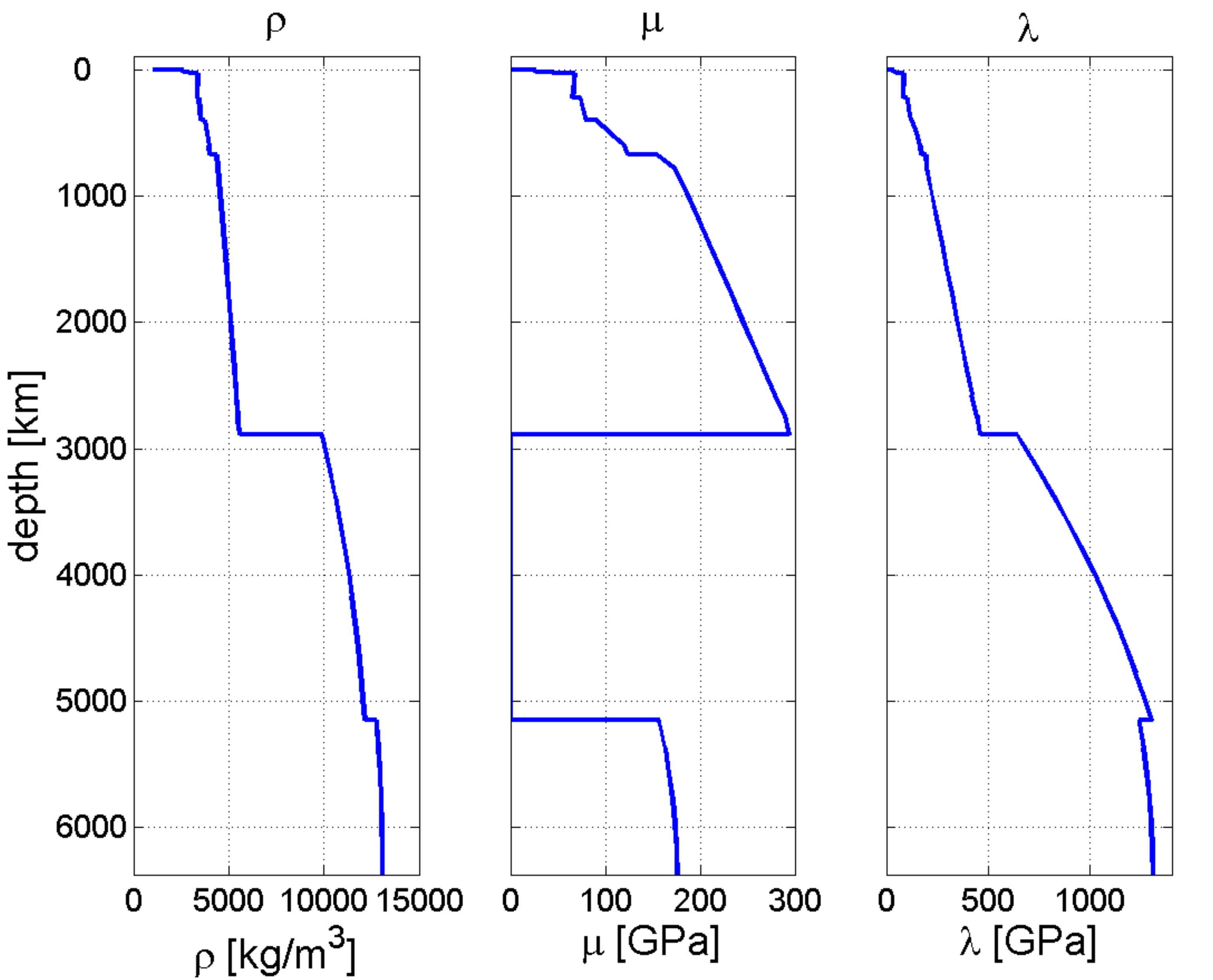

ρ
μ
λ
0
1000
2000
3000
4000
5000
6000
depth [km]
0
5000
10000
15000
ρ [kg/m3]
0
100
200
300
μ [GPa]
0
500
1000
λ [GPa]

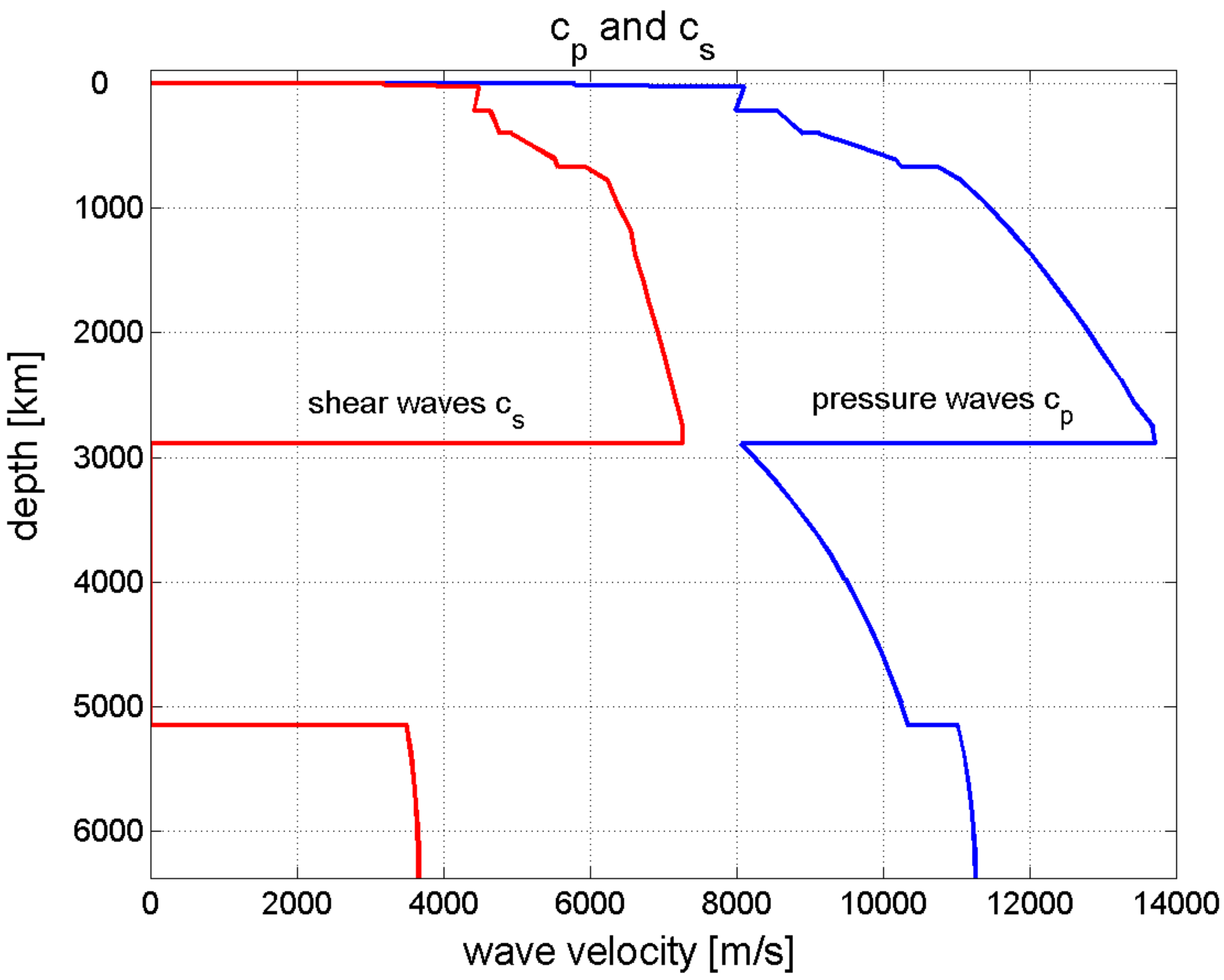

c_p and c_s
0
1000
2000
3000
4000
5000
6000
depth [km]
shear waves c_s
pressure waves c_p
0
2000
4000
6000
8000
10000
12000
14000
wave velocity [m/s]

Elapsed time: 46 sec

Elapsed time: 92 sec

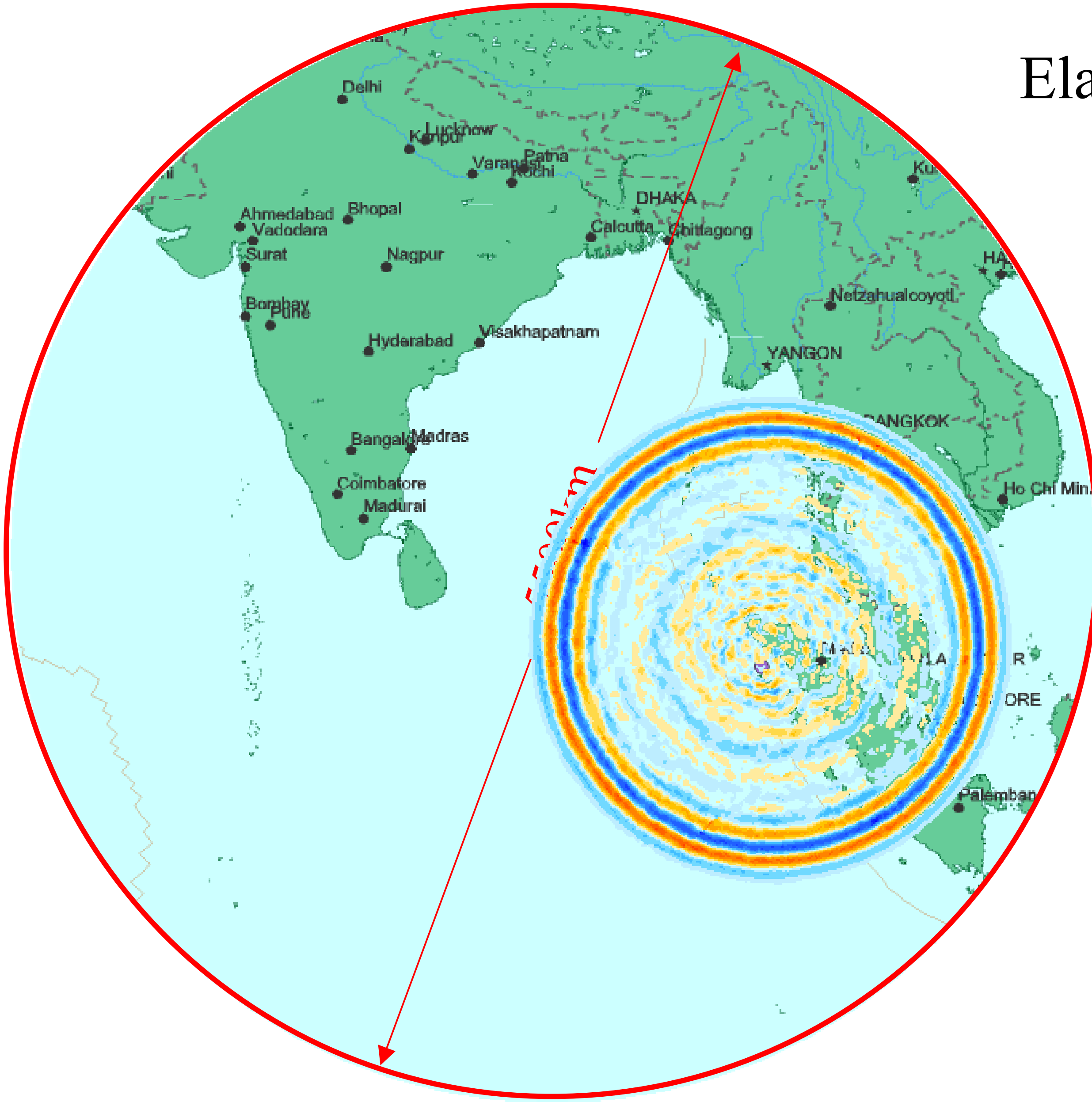

Elapsed time: 138 sec

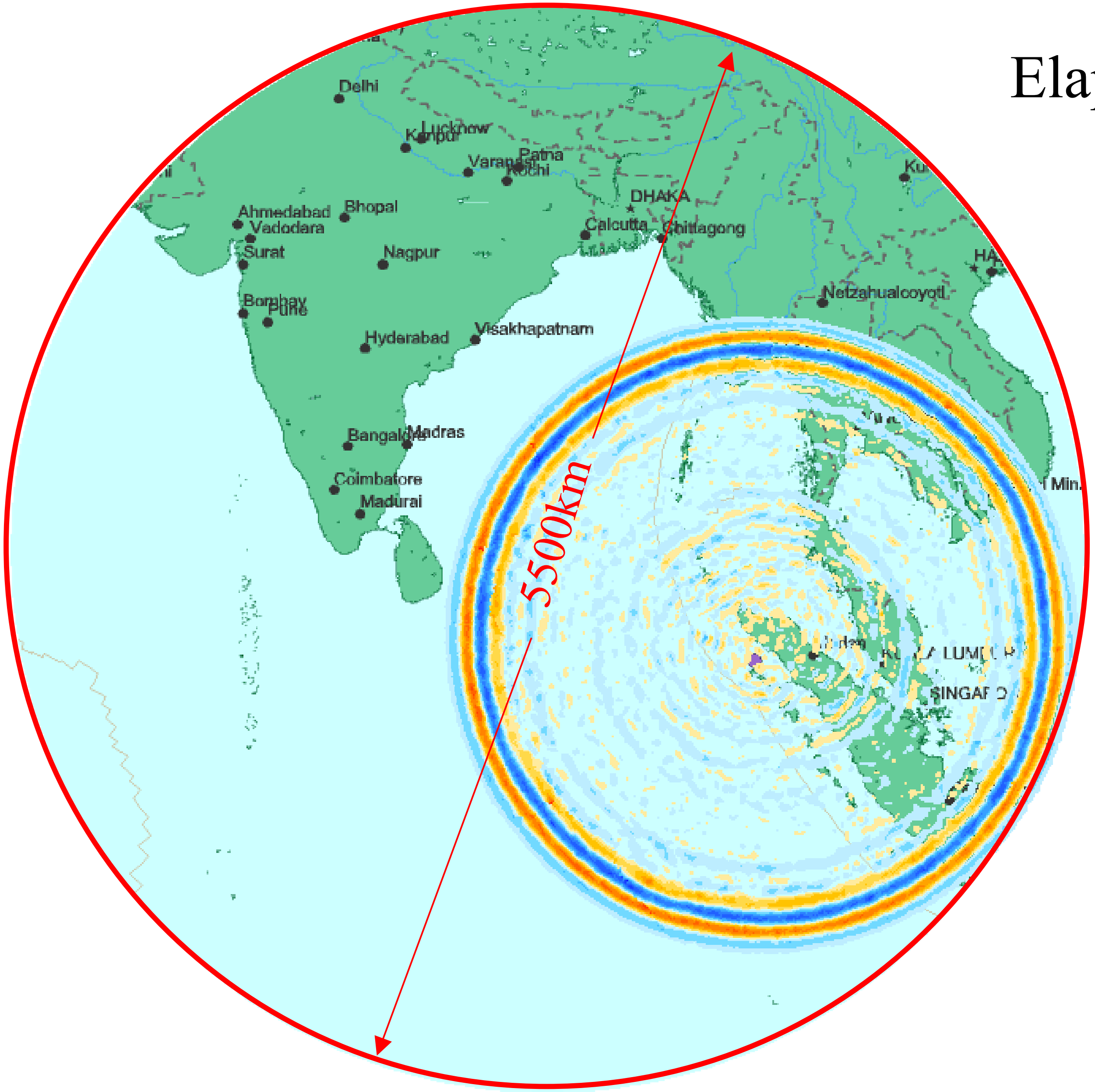

Elapsed time: 184 sec

Elapsed time: 230 sec

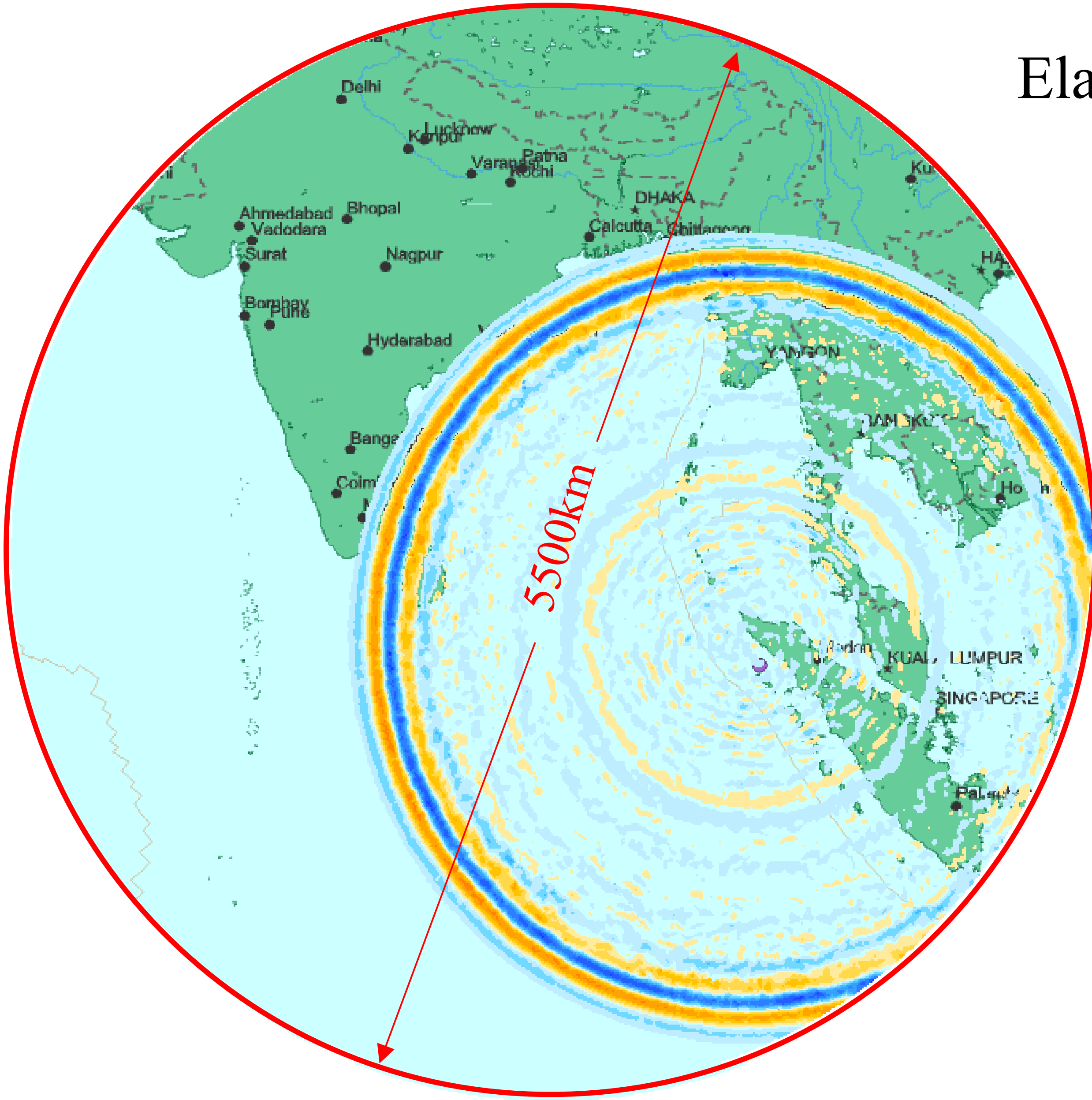

Elapsed time: 276 sec

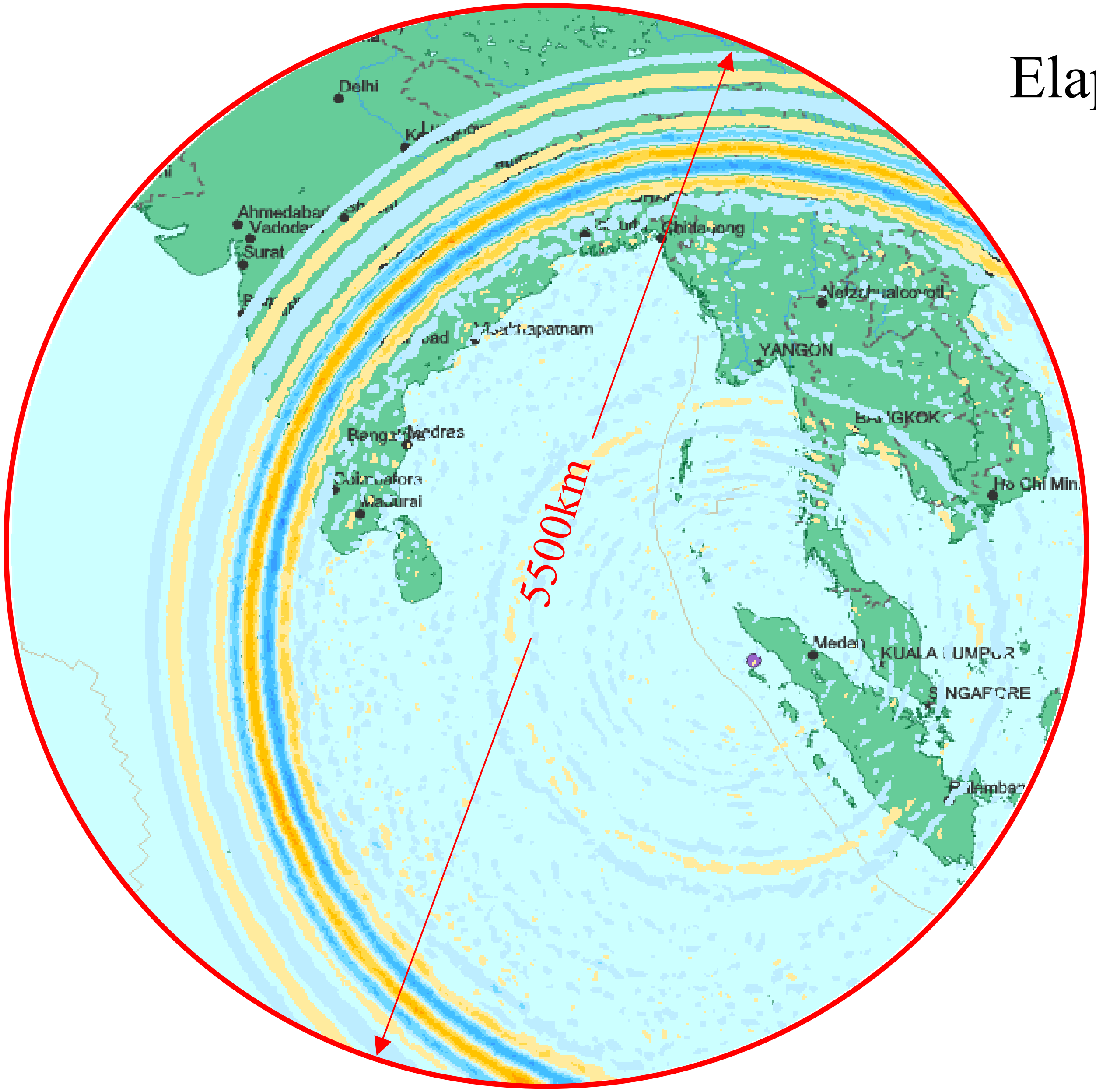

Elapsed time: 322 sec

Elapsed time: 368 sec